THE DESIGN AND CONSTRUCTION OF A CRYOSTAT FOR THERMAL BATTERY INVESTIGATIONS

-

BRETT MATTHEW SWANN

A DISSERTATION SUBMITTED TO THE SCHOOL OF ELECTRICAL, ELECTRONIC AND COMPUTER ENGINEERING,

IN FULFILMENT OF THE REQUIREMENTS FOR THE DEGREE OF MASTER OF SCIENCE IN ENGINEERING, FACULTY OF ENGINEERING,

UNIVERSITY OF KWAZULU-NATAL

18 MARCH 2011

SUPERVISOR: DR A. L. LEIGH JARVIS

EXAMINERS COPY

I ..... declare that

1) The research reported in this thesis, except where otherwise indicated, is my original work.
2) This thesis has not been submitted for any degree or examination at any other university.
3) This thesis does not contain other persons' data, pictures, graphs or other information, unless specifically acknowledged as being sourced from other persons.
4) This thesis does not contain other persons' writing unless specifically acknowledged as being sourced from other researchers. Where other written sources have been quoted, then:
    a) their words have been re-written but the general information attributed to them has been referenced;
    b) where their exact words have been used, their writing has been placed inside quotation marks, and referenced.

Signed:

As the candidate's supervisor, I have approved this dissertation for submission.

Name: .....

Date: .....

Signature: .....

Acknowledgements

There are many people of who have aided me throughout my masters whom I'm indebted to:

- Dr Leigh Jarvis who whilst guiding me through my research has gone far beyond the requirements of a supervisor on many an occasion
- My Mother, having supported me through my years of study and providing an abundance of meals whilst I was lost in realm of research
- Jonathan Archer and Peter Adigun, fellow post-grads and friends who've assisted me on countless occasions
- The university technical staff, in particular Anthony Lester, Dharma Moodley and Johan Swanepoel
- Colombo Fine Beverage Co. for providing many a cappuccino to fuel much of my dissertation
- The NRF who've funded me throughout my research.

S. D. G.

Abstract

A test cryostat was constructed to investigate the potential of a locally made thermal battery. A thermal battery is proposed to be a useful component in the construction of future superconducting fault current limiter (SFCL) systems. The heat generated from a SFCL under quench conditions can be conducted into a solid nitrogen thermal battery. This is an alternative to using a liquid cryogen which on evaporation would form a highly non-conductive vapour layer around the SFCL and could be potentially explosive. The relevant heat transfer mechanisms for cryostat design were analyzed to ensure that the cryostat was capable of solidifying nitrogen and thus be used as a thermal battery. The experimental stage was ultimately capable of reaching a temperature of 40 K. Using a resistor to mimic the normal state of a superconductor, the performance of the thermal battery was determined by subjecting it to transient thermal events. The effect of solid nitrogen crystal size was investigated by performing pulse tests on solid nitrogen formed at different rates. It was found that slowly formed solid nitrogen performed better and stabilised the resistor's temperature more quickly. The phenomenon of 'dry-out' was also investigated for different formation rates by subjecting the solid nitrogen to multiple heating pulses. It was found to become very significant after the first pulse when using quickly formed solid nitrogen, but did not manifest in slowly formed solid nitrogen.

Table of Contents

Acronyms

Symbol	Description
FCL	Fault Current Limiter
SFCL	Superconducting Fault Current Limiter
HTS	High Temperature Superconductor
MgB_2	Magnesium Diboride
RLI	Reactive Liquid Infiltration
OFHC	Oxygen Free High Conductivity
ETP	Electrolytic Tough Pitch
PD	Phosphorus Deoxidised
1G	First Generation
2G	Second Generation

Table of Variables

Variable	Description
k_{GL}	Ginzburg- Landau parameter
ξ	Coherence length
λ_P	Penetration depth
Z	Z-ratio value
R_T	Measured PT100 resistance
R_{273K}	PT100 resistance at 273K
$R_{4.2K}$	PT100 resistance at 4.2K
$\dot{q}_{cond}$	Heat flow due to conduction through a solid
λ_T	Thermal Conductivity
A	Area
L	Length
$\dot{q}_{gas}$	Heat flow due to conduction through a gas
$\overline{\lambda}$	Average thermal conductivity
d	Plate separation distance
P	Pressure
T	Temperature
a_0	Accommodation coefficient
k_g	gas constant, dimensionless
E_b	Energy density flux for a blackbody
σ	Stefan-Boltzmann constant
ε	Surface emissivity
$\dot{q}_{rad}$	Heat flow due to thermal radiation
E	Combined surface emissivity
ρ	Electrical resistivity
λ_r	Radiation wavelength
$\dot{q}_{MLI\_shield}$	Radiative heat flow when using a MLI shield
N	Number of layers of superinsulation
$\dot{q}_{rad\_shield}$	Radiative heat flow when using a thermal shield

List of Figures

List of Tables

1 Introduction

A thermal battery, also known as a heat capacitor, is a material added to a cryogenic system to increase its heat capacity for the purpose of improving the systems thermal stability. Selecting a material which has phase changes in the temperature region of operation will improves the thermal stability through the inclusion of the relevant latent heats. Thermal batteries are of particular interest in the field of Superconducting Fault Current Limiters (SFCL). The SFCL is a promising and effective approach to limiting fault currents and is currently under active research. An issue with SFCLs is that when the superconductor quenches and returns to the normal state, it becomes resistive and generates heat. Preventing this from damaging the superconductor is a problem for which the thermal battery is a promising solution.

1.1 Problem Statement and Chapter Overview

This dissertation deals with the design and construction of a cryostat to be used in testing of thermal batteries. This has application in Superconducting Fault Current Limiters because the heat generated during quench is of major concern. The use of a solid nitrogen thermal battery is an attractive solution to absorb the heat. This research looks to refine the current understanding of a solid nitrogen thermal battery's performance by better understanding how the cooling rate during solidification affects the thermal contact resistance between the solid nitrogen and contact surfaces.

In Chapter 2 the design, assembly and testing of the cryostat are discussed. It begins with heat transfer theory, followed by relevant sample calculations.

In Chapter 3 the experimental procedures adhered to in testing the performance of the thermal battery are outlined.

In Chapter 4 the results obtained from the experimentation are presented.

In Chapter 5 some additional experiments and possible methods to improve the thermal contact for a solid nitrogen battery are proposed.

1.2 Thermal Batteries

A thermal battery makes use of a materials specific heat capacity to improve the thermal stability of a system.. Different substances can be used for the thermal battery. Figure 1.1 provides a comparison between the volumetric specific heat capacities of several materials. Nitrogen's higher heat capacity and latent heats in this temperature range make it the most attractive choice for the present application.

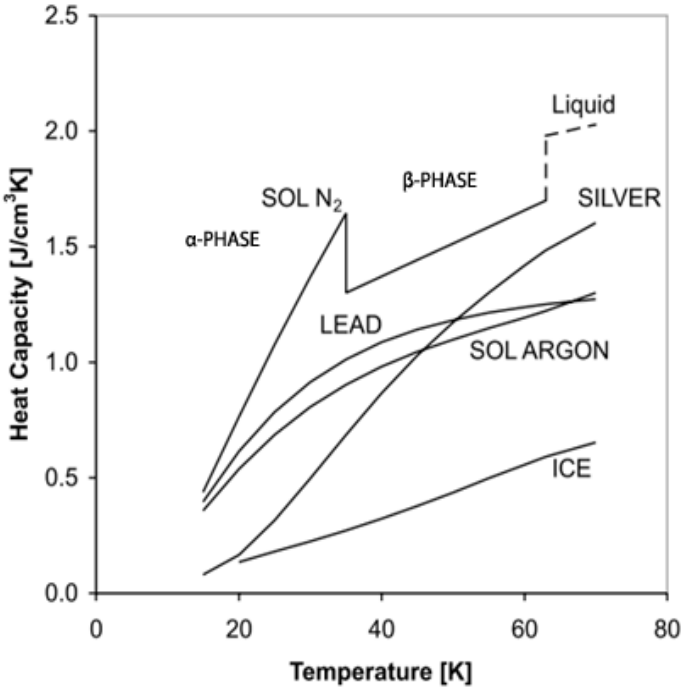

Figure 1.1 Volumetric Heat Capacity vs. Temperature for several materials [1]

It is important that the thermal contact resistance between the thermal battery and the system be minimised. This contact resistance significantly impacts the thermal battery's ability to suppress thermal transients.

1.2.1 Use with SFCLs

A key issue to be overcome with SFCL's is the heat generated during a fault. When a fault occurs and the current has exceeded the critical current[1] and the superconductor quenches[2] and returns to its normal state[3], becoming resistive. This generates a significant amount of

[1] The critical current of a superconductor is the highest current which can flow through it, after which its superconducting characteristics cease.

[2] A superconductor quenches when the current flowing through it exceeds its critical current and it returns to the normal state.

[3] The normal state is when a superconductor does not exhibit superconducting characteristics.

heat due to Joule heating, $P = I^2R$. In practice superconductors do not heat uniformly. If the superconductor is not homogeneous, “hot spots” to develop and the temperature of these regions can rise rapidly. The occurrence of hot spots raises the importance of dealing with the heat generated during a fault because they increase the probability of damage to the superconductor and its supporting materials.

A solution to the above problem is to use either a liquid or solid cryogen as a thermal battery or heat capacitor. Its function is to improve the thermal stability of the system during transient heating by providing a substance with a large heat capacity, which is in contact with the superconductor. Liquid cryogens are vaporised when heated above the boiling point and the expansion ratio is a crucial consideration. Liquid nitrogen’s expansion ratio on boiling is 1:694 and could lead to the vessel exploding if it is not equipped with pressure release valves [2 - 5].

1.2.2 Solid Nitrogen

There has been much interest in the use of solid nitrogen as a thermal battery due to its high specific heat capacity and heat of fusion (melting point: 63.15 K). Additionally, there is the significant latent heat of nitrogen's α-β solid phase change occurring at 35.6 K.

There are problems in solid nitrogen’s application which need to be addressed. Any spaces between the solid nitrogen and the superconductor will increase the thermal contact resistance and thus reduce the effectiveness of the thermal battery. It has been found that the rate at which the nitrogen is cooled during solidification affects the thermal contact considerably [6]. Rapidly formed solid nitrogen which was found to perform poorly has been described as porous, and visually appears to be “fluffy” [4][6]. An experiment was performed to visually observe this and images can be seen in Figure 1.2. The rapid temperature change during solidification causes crystal growth to occur at multiple nucleation sites. The solid appears somewhat opaque because of the vast number of inter-granular defects which form in the crystal. Slowing the rate of cooling reduces the number of these defects. Solid nitrogen contracts when cooled, which is an additional reason for the thermal contact to be degraded upon cooling to its operating temperature.

Figure 1.2 Solid Nitrogen rapidly produced by pumping on the liquid

A second area of concern is a phenomenon known as “dry-out”. This is a phenomenon that is observed after the solid nitrogen has been subjected to a number of thermal disturbances, and data suggests that the thermal contact between the solid nitrogen and sample deteriorates. The number of disturbances is believed to be related to the heat flux through the solid-nitrogen-superconductor interface, and that there is a minimum heat flux below which the phenomenon does not occur [6].

1.2.3 Hybrid Refrigerants

There have been some promising results in the use of hybrid refrigerants to improve the thermal contact between solid nitrogen and the superconductor. Some of these results show the addition of small quantities of neon in the form of gas and liquid increases the thermal conductivity by 50% [7 - 9].

The mechanism by which this improvement occurs is not well understood. Micro-gaps are likely to develop as the solid nitrogen is cooled leaving vacuum spaces between the solid nitrogen and the superconductor. The neon gas could diffuse through the nitrogen and fill these spaces, improving conduction.

1.3 Cryostat Design

A cryostat is a vessel which is designed specifically to be used at low temperatures, either for the operation of electronics or for measurements. They can be designed in a variety of geometries, yet most have roughly a cylindrical shape. Types of cryostats (grouped by the method of cooling) include:

- Dipper (Liquid Cryogen)
- Cryocooler
- Liquid flow
- Gas flow

All-purpose cryostats are not sold commercially because cryostats can vary significantly in their design depending on their application. However, application specific and custom cryostats are available.

In the design of a cryostat, the following questions need to be considered:

- What measurements or functions will the cryostat need to perform?
- Will a liquid cryogen be used or a cryocooler?
- What temperature will it need to operate at?
- How accurately must the temperature be controlled?
- Will mechanical or optical access be required?
- Will there be high magnetic fields?

A thermal battery test cryostat needs to operate below the cryogen's melting point, which in this case is nitrogen's (T_m (N_2) = 63.15 K). Temperature control is important for experimentation, especially where cooling rates are to be controlled. A cryocooler is used for this purpose because of the flexibility it offers for temperature range and control. Whilst optical and mechanical access and high magnetic fields are not required, inlet pipes are needed to pump in liquid nitrogen. The purpose of the apparatus, of which the cryostat is an important component, is to perform transient heating experiments on the thermal battery to investigate how the formation method of solid nitrogen influences its performance.

1.3.1 Thermal Contact Resistance

Thermal contact resistance is the inverse of thermal contact conductance. On the microscopic level, no surface is flat. Each surface has many asperities, i.e. peaks and troughs. Most of the techniques used to produce engineering surfaces have been experimentally shown to follow a Gaussian distribution of heights [10][11]. When two surfaces are joined, these peaks and

troughs do not fit perfectly together, and the overall contact area is a small percentage of the apparent contact area.

Factors which influence the contact resistance depend on how the join is made and what interstitial material is present. Joins with the lowest contact resistance are welded joins, solder joins, followed by epoxy, varnish, thermal grease, and finally pressure joins [12]. Oxide layers formed on the surfaces before they are joined add to the contact resistance [13].

If a pressure join is made where there is either no interstitial material or it has a low thermal conductivity, the resistance of the join is primarily dependant on the pressure of the join and not on the 'apparent' contact area. Pressure joins can be improved by using thermal grease as the interstitial material. For cryogenic joins, Apiezon N grease performs exceptionally well. Figure 1.3 shows the improvement to contact conductance of a copper-to-copper join with using Apiezon N grease at liquid helium temperatures. [14]

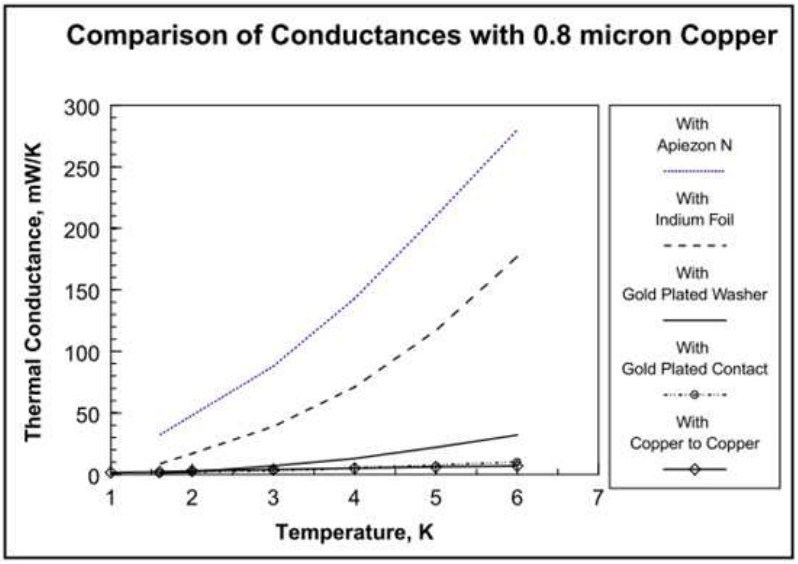

Figure 1.3 Comparison of Copper contacts for different interstitial materials [14]

It is possible to deal with the thermal contact resistance rigorously based on contact mechanics and thermal models, but this is generally unnecessary in cryostat design [11][15]. Thermal conductance can generally be estimated using Figure 1.4.

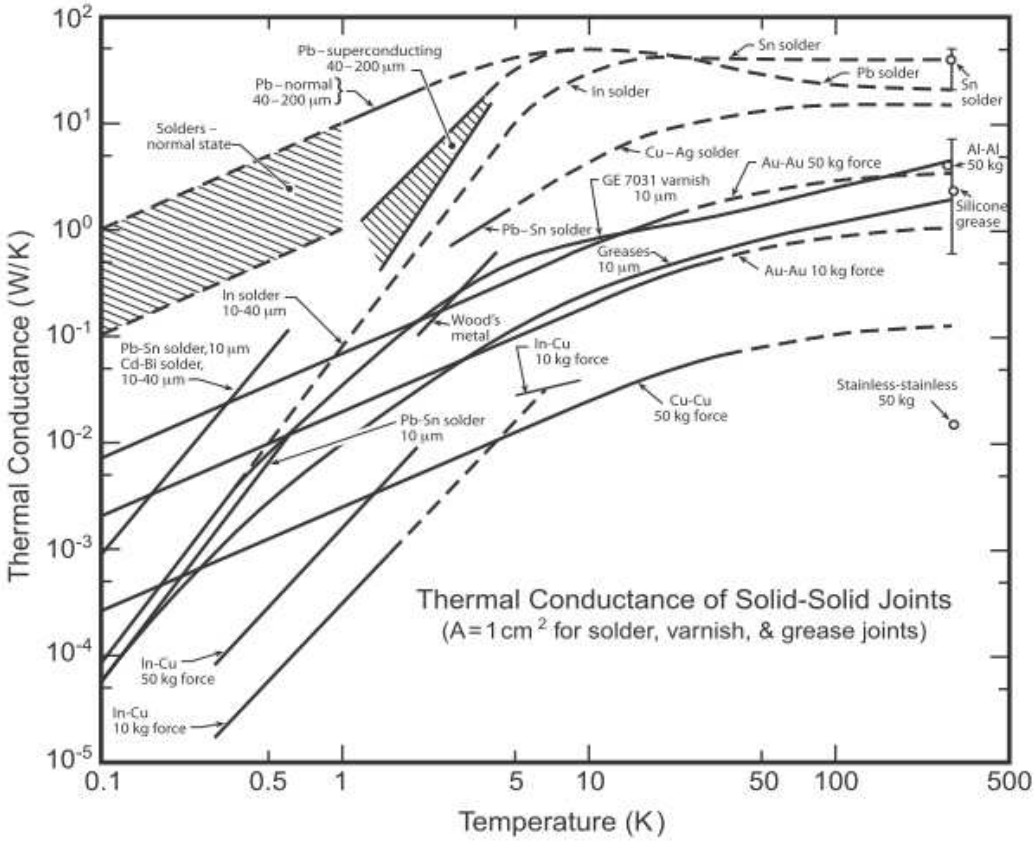

Figure 1.4 Thermal Conductance for Solid-Solid Interfaces [12]

The data shown in Figure 1.4 shows the benefit of making permanent joins instead of pressure joins. Consequently cryostats should, where possible, be designed with permanent joins if high thermal conductance is desired. In the instances where it is not possible to make a permanent join, such as connections to the cold finger of a cryocooler, the use of thermal greases and gold plating of the contacts is the next best option.

1.4 Superconductivity

Superconductivity is a quantum phenomenon which can be observed on a macroscopic level. It is concisely described as follows:

> *"An electronic state of matter characterised by zero resistance, perfect diamagnetism, and long-range quantum mechanical order"* [16]

The above characteristics indicate the onset of the superconducting state. Zero (dc) resistance was the first to be observed with Mercury in 1911 by H. K. Onnes who noticed a sharp drop in resistance at 4.2 K [17]. When an ac current flows through the superconductor a frequency dependant resistance appears which is only significant at higher (microwave) frequencies.

As the superconductor sets up screening currents near its surface to shield out magnetic fields, it exhibits perfect diamagnetism, assuming the fields are below the critical field (H_c). This is known as the Meissner Effect. The setting up of the screening currents occurs on transition into the superconducting state. Magnetic fields penetrate the superconductor to a depth known as the London penetration depth.

Superconductors have both a critical electrical current and critical magnetic field, each of which when exceeded returns the superconductor to the normal state. These values are temperature dependant, decreasing as one approaches a critical temperature or magnetic field and can be represented in a 3D phase diagram as shown in Figure 1.5.

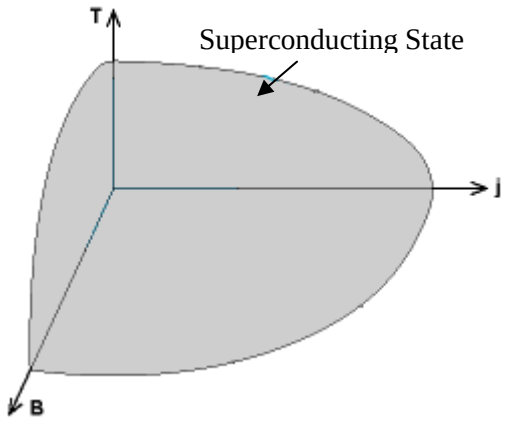

Figure 1.5 Simplified Superconductor 3D Phase Diagram[18]

There are two classes of superconductors, Type I and II, which behave differently to applied magnetic fields. The difference in the behaviour of the two classes is determined by the so-called Ginzburg-Landau parameter (k_{GL}), defined as the ratio of the 'penetration depth',

λ_P, and 'coherence length', ξ, shown in Equation 1 is known as the Ginzburg–Landau parameter. A superconductor is Type I if $k_{GL} < 1/\sqrt{2}$, and Type II if $k_{GL} > 1/\sqrt{2}$.

$$k_{GL} = \frac{\lambda_P}{\xi} \tag{1}$$

Type I superconductors have a single critical field value beyond which it returns to the normal state. Type II superconductors are capable of a mixed state that allows a mixture of superconducting and normal regions. Due to energy reasons a magnetic field can penetrate a Type II superconductor forming magnetic vortices. This occurs when the applied field is between its first critical field value (H_{c1}) and second critical field value (H_{c2}). The value of H_{c2} is always higher than H_c, and in turn the critical current for Type II superconductors is generally greater than Type I. The M (H) phase change is shown in Figure 1.6 [19]

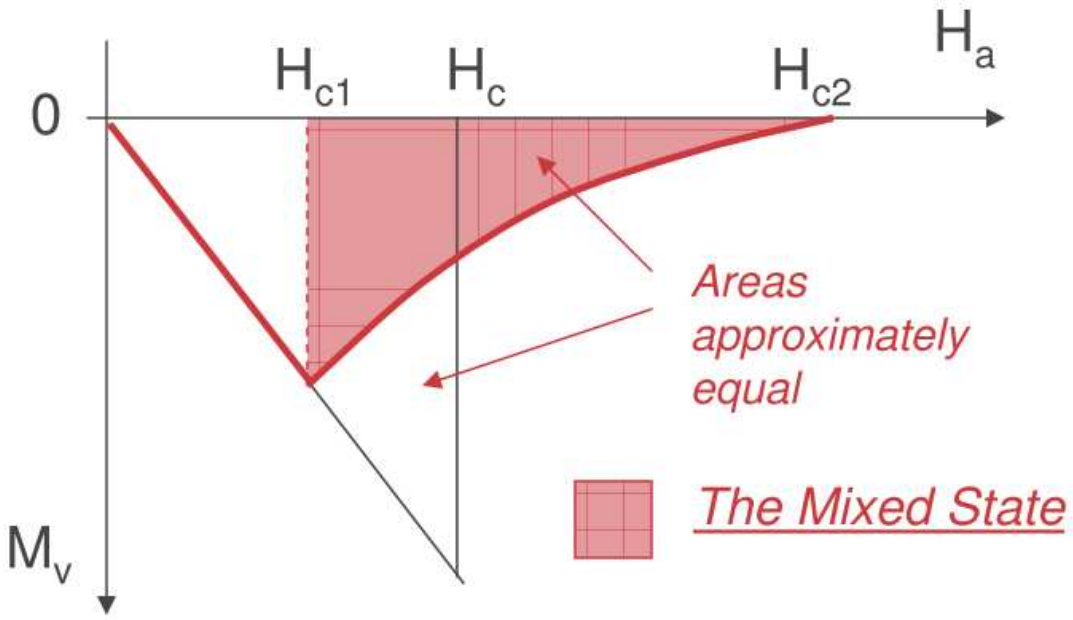

Figure 1.6 M (H) Phase Diagram [16]

1.5 Fault Current Limiters

1.5.1 Faults in Power Distribution Systems

There are two types of faults in power systems, active faults and passive faults. An active fault is classified as being when the fault current is flowing from one phase to another, from a phase to neutral or from a phase to earth. Causes of active faults include physical bridging of the phases through a conductive medium such as digging machinery striking the conductors, infrastructure damage from heavy weather or after/during theft of conductors.

Other causes can be more gradual, such as partial discharges in a void of insulation between phases. Over time the insulation degrades and a large fault occurs. [20]

Passive faults are those which place the power system under stress, which can eventually lead to an active fault. Causes of passive faults include: overloading, overvoltage, under frequency, and power swings. [20]

Fault current levels caused during active faults can be very large and need to be limited quickly to avoid serious damage to the infrastructure such as transformers due to heating and vibrations, as well as fires from the overheating of conductors. Protection is needed for each phase.

1.5.2 FCL Technologies

Fault current limiting is becoming an increasingly active field of research as fault currents levels rise with grid expansion and interconnection. It finds application in both AC and DC systems. Present fault interception technologies – including high voltage switchgear, series reactors, and explosive fuses – have disadvantages ranging from the expense for switchgear, losses associated with series reactors, and maintenance time on changing explosive fuses. Switchgear is a practical solution, but presently the technology has an upper limit of about 80 kA. This limit is quickly being reached and it is believed that fault currents in some systems are around ±60 kA [21]. Fault current interception and limiting technologies currently being researched include:

- Resistive Superconducting FCLs [21]
- SFCL Transformers [16]
- Solid-state FCLs [16]
- Smart Current Interception Devices (ABB I_s Limiter) [23]
- Magnetic FCLs [24]
- Interphase Power Controllers [25].

1.5.3 Superconductive Fault Current Limiters

Interest in the area of SFCLs has been growing as methods of manufacturing long High Temperature Superconductor[4] and MgB_2 superconducting wires/tapes have improved, and their costs have decreased. Resistive SFCL's comprise of either long lengths of superconducting wire, or bulk superconductor pieces, and make use of the superconductor's

[4] For the purpose of this dissertation, a High Temperature Superconductor is viewed as being a material with a critical temperature greater than 30 K.

critical current to limit the fault current (quench). During quench the superconductor becomes resistive, dynamically adding impedance to the system and hence reducing the fault current level. This can be used in conjunction with switchgear, as the current can be limited by the SFCL to a level that the switchgear is capable of intercepting the fault without damage [16].

The SFCL is an attractive solution to deal with fault currents. They have minimal losses during operation, quick response time to fault conditions, and potentially fast recovery time[5] [21]. Simulation methods have shown that SFCL's improve power system stability under transient conditions and improve power quality [26].

1.5.4 Superconductor Material for SFCL's

There is a significant amount of research activity in the area of High Temperature Superconductor (HTS) FCL's. HTS materials have the advantage that they can be used in either liquid nitrogen or a cryocooler. Nexans SuperConductors, based in France, are offering the first commercially available HTS FCL for medium voltage systems (15kV) using High T_c monofilar BSCCO 2212 bulk material coils [16].

The material for HTS FCL's comprise of either bulk material [27] or first generation (1G) or second generation (2G) HTS wire/tape [28]. 1G tape, which is commonly fabricated by the 'Powder (superconductor) in Tube (silver) method', can be produced in long lengths of wire/tape. 1G wire is expensive to produce due to the use of large amounts of silver in the manufacturing process. They also suffer from intergranular weak-link behaviour which reduces the critical current by more than an order of magnitude. 2G HTS material is becoming more attractive as it is significantly cheaper to produce (2G wire was about ¼ of the price of 1G wire in 2010), but there are challenges in manufacturing long lengths of the wire [21].

Another FCL superconductor of interest is Manesium Diboride (MgB_2) whose superconducting properties were discovered in 2001 [29] [30]. MgB_2 is a promising superconductor as it is relatively cheap, easy to manufacture and has a low density [30]. With a critical temperature of 39 K it cannot operate in liquid nitrogen but it is economical for it to be cooled by either a cryocooler or liquid hydrogen. It has several benefits over HTS; namely, smaller anisotropy and it is less inclined to problems with weak-links [31].

[5] The recovery time is the amount of time it takes after the fault has occurred for the superconductor to return to the superconducting state.

The relative ease and low cost of manufacturing lends itself towards long MgB_2 wires being produced, which finds application in numerous areas.

There are some problems with MgB_2 that researchers are currently attempting to solve. The critical current density for a pure sample was found to be roughly 35 kA/cm^2 in 2002 [30]. This is much lower than that required for motor and transformer applications and can be improved by intentionally adding defects to pin the magnetic vortices and prevent them from moving [30]. More recent studies on MgB_2 wires produced by Hyper Tech Research Inc., with a CuNi sheath, Nb barrier and SiC doping, show the critical current density to be in the region of 460 kA/cm^2 [32].

High quality samples of MgB_2 are currently being produced at the University of Kwa-Zulu Natal and will ultimately be used in a locally made SFCL. The technique used to produce the samples is the recently published Reactive Liquid Infiltration (RLI) technique that allows for bulk polycrystalline pieces to be produced that have a high density [33]. In this technique liquid magnesium and boron powders are reacted in a sealed metallic vessel with inner walls sheathed in Tantalum or Molybdenum. The reaction occurs at a temperature between 750 ºC and 950 ºC. It is recommended to use a bulk piece of Magnesium as turnings would need to be compacted because free space inside the vessel needs to be minimised. The introduction of oxygen into the system results in the formation of MgO which negatively affects the superconductivity of the MgB_2 sample.

1.5.5 The Problem of Hot Spots

Hot-spots occur when a region of the superconductor becomes normal before the bulk of superconductor does. Hot spots are problematic when the superconductive material is not homogeneous. This is primarily due to the critical current of that region being lower because of defects and impurities. A significant amount of heat can be generated in a hot-spot region before the bulk of the superconductor becomes normal. Bulk superconductors are at risk of cracking due to thermal stresses when the “hot spot” regions expand as their temperature increases. Superconductive films and wires have been known to be damaged at higher temperatures as seen in Figure 1.7.

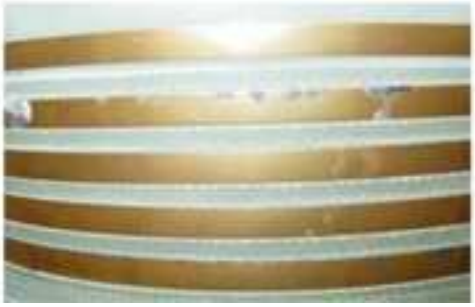

Figure 1.7 HTS Tape Damaged from Quench [34]

1.6 Thermometry

It is important to measure temperature accurately, both for experimentation purposes and temperature control. The choice in type of thermometer is governed by a number of factors which include: accuracy, reproducibility, interchange-ability, calibration drift, and use in magnetic fields. Response time of the sensor is particularly important in this application.

1.6.1 Platinum Resistance Sensors

An summery of several popular thermometers and the temperature range which they can be used in is below in Table 1. High cost is often unavoidable for accurate low temperature thermometers.

Table 1 Temperature Range and Cost of Several Popular Thermometers [12]

Type	Calibration	Temperature Range	Cost
Platinum Resistance (uncalibrated)	No	77-800 K	Low
Platinum Resistance (calibrated)	Yes	22-77 K	High
Germanium Resistance	Yes	0.05-100 K	High
Silicon Diode	Yes	1.4-475 K	High
Type E Thermocouple	No	3-1274 K	Low, DC voltage measurement
Capacitance Sensor	Yes	1-290 K	Medium, Capacitance measurement

The PT100 is a platinum resistance thermometer with a positive temperature coefficient which is widely used both in industry and R&D. Uncalibrated PT100's are generally only used down to about 70 K, the lower limit of the standard temperature/resistance tables, whilst calibration allows them to be used down to around 15K. The need for calibrating the PT100 at these temperatures is that the resistance of the thermometer at very low temperatures is dominated by the impurity content of the platinum, a property which varies from one PT100 to another. At these lower temperatures the sensitivity of the thermometer

falls off significantly as the resistance drops to a few ohms. It is, however, an attractive option because of its low cost and high reproducibility.

Excitation currents for the thermometer are often in the order of milliamps, in order to reduce self heating of the thermometer which would otherwise affect the measurement. At lower temperatures this can be troublesome if the noise floor of the system is high.

PT100 thermometer resistance measurements should be performed using the 4-lead resistance measurement technique rather than the 2-lead technique. A significant source of error from the 2-lead technique is the lead resistance, especially if phosphor-bronze wiring has been used to minimise the heat flow because it has a much higher resistance per meter than copper. As shown in Figure 1.8 the 4-lead technique connects the PT100 to the current source with 2 of the leads, and voltmeter with the other 2 leads. [35]

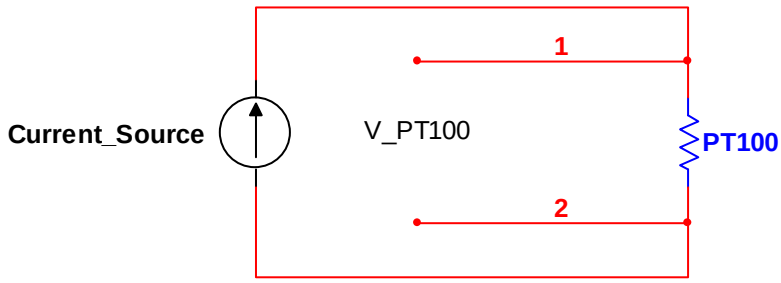

Figure 1.8 4-lead measurement technique

Additional considerations when using PT100s include the Seebeck effect and shielding.

1.6.1.1 Manual Calibration Techniques

PT100's can be manually calibrated against any pre-calibrated thermometer. There must be minimal thermal resistance between them so that the uncalibrated PT100 closely coincides with the temperature of the calibrated thermometer. Several points can be taken in the desired temperature range, and a greater number of points are taken at lower temperatures as the sensitivity of PT100's is falls off at lower temperatures (Figure 2.20). The dimensionless sensitivity of PT100's is seen in Figure 1.9 where it is compared with that of several thermometer types. On the figure, *O* represents the output unit of the thermometer, and *T* the temperature. If the two thermometers are made of different materials with different specific heat capacities and different masses, the temperature should be kept constant for a period of time before the measurement is taken to ensure they are in thermal equilibrium. The accuracy of the calibration is limited to that of the calibrated reference thermometer, and can be reduced significantly if care is not taken to correctly mount both thermometers, thermally anchor the wiring to the thermometers, and minimise self heating.

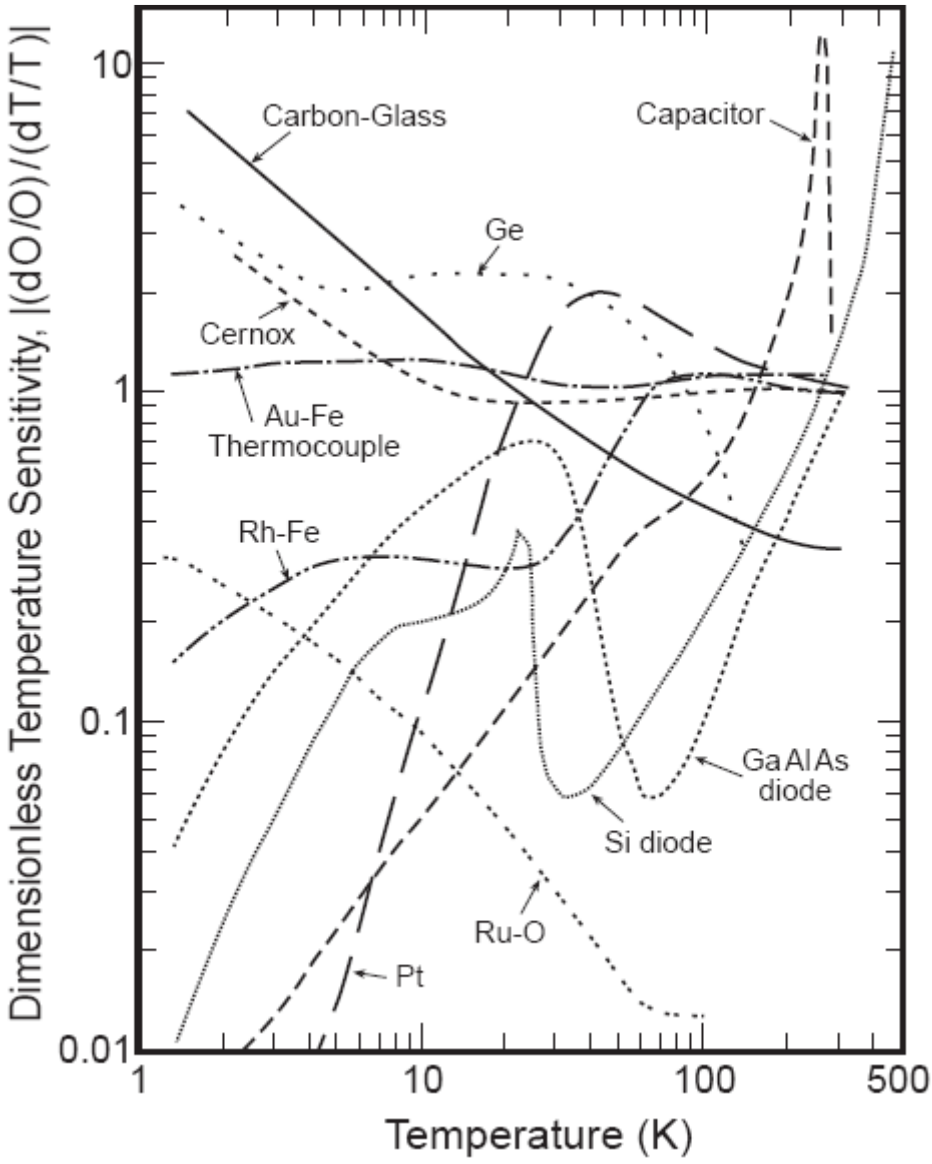

Figure 1.9 Temperature vs. Dimensionless Sensitivity Graphs for thermometers [12]

1.6.1.2 Z-ratio Calibration

This is a simple and effective method for calibrating PT100's. Calibration is done by measuring the resistance of the PT100 at liquid helium temperatures (4.2K) and at the triple point of water (273K). The resistance measurement at 4.2K givens an indication of the impurity content of the platinum so that corrections can be made. Equation 2 below is used to find a Z-ratio value which corresponds to a specific temperature. This value is compared to those on the Z-ratio table which contains z-ratio values and temperatures. The temperature is found by interpolating between points on the table.

$$Z = (R_T - R_{4.2K})/(R_{273K} - R_{4.2K}) \quad (2)$$

The error when using this method is approximately ±25 mK in the range of 30 K, and ±120 mK at 12 K.

2 Cryostat Development

Developing a cryostat is a specialized process which requires knowledge of heat transfer processes and of cryogenic techniques. To reach the temperatures desired, either liquid cryogens or cryocoolers are used. The cryostat is designed around the method of cooling, adhering to certain design requirements and meeting the cryostat's purpose.

Heat transfer into the cryostat needs to be carefully considered in its design so that its desired minimum operating temperature is attainable. It also has a significant impact on the financial operating cost of cryostat a when using liquid cryogens as additional heat sources will cause the cryogen to boil off at a faster rate. For a cryocooled Superconductive Fault Current Limiter, minimising the heat flow into the cryocoolers stages will maximise the cooling power and allow the cryocooler to re-cool the superconductor faster after it has quenched a fault. Considering the relevant heat transfer mechanisms for this design (conduction and radiation) and the areas where they apply will highlight how easily heat transfer can be underestimated.

The experimental stage of the thermal battery test cryostat will need to be able to reach the melting point of the cryogen used (63.15K for nitrogen). This stage must also be capable of storing the cryogen prior to its solidification and be equipped with appropriate cryogen transfer lines. The chief purpose of the cryostat for this research is to test the thermal battery, and probe the heat dynamics.

2.1 Theory of Heat Transfer

2.1.1 Heat Conduction - Solids

The conduction of heat through solids is a fundamental aspect in this design and is well established in thermodynamics literature. Every physical link to the experimental stage, other than the cryocooler, is an additional path for heat to flow in from another part of the cryostat or its environment. Fourier's Law of thermal conduction flux per unit area and time for an element with uniform cross sectional area is given by

$$\dot{q}_{cond} = \lambda_T(T)\, A\ dT/dx = (A/L)\ \int_{T1}^{T2} \lambda_T(T)\, dT, \qquad (3)$$

where $\lambda_T\,(T)$ is the temperature dependent thermal conductivity; A is the cross-sectional area, L is the length between T_1 and T_2, and dT/dx the temperature gradient between T_1 and T_2,

Thermal conductivity integral tables can be used to simplify the calculation and are found in thermodynamics and cryogenic engineering handbooks. Calculating the thermal conductivity integral between any two temperatures can be done by subtraction of the values on the table.

2.1.2 Heat Conduction - Gases

There are two considerations to inspect of heat-conduction in gases in cryostat design, namely, (i) vacuum insulation and (ii) heat exchange apparatus. Heat conducted through a gas is difficult to calculate accurately. There are two different regimes which describe the way heat is conducted, hydrodynamic and free-molecule. Classifying the heat conduction into either of these regimes is done by comparing the 'mean free path'[6] of the gas's molecules with the distance separating the hot and cold surfaces.

If the mean free path of the gas molecules is much less than this separation distance then the collisions between the gas molecules cause the heat transfer to be dependent on the thermal conductivity of the gas. This is known as the hydrodynamic regime. In this case heat conduction is independent of pressure. For two parallel plates the heat conduction flux per unit time is described by

$$\dot{q}_{gas} = \bar{\lambda} A \Delta T/d, \qquad (4)$$

[6] A gas molecule's mean free path is defined as follows: $l = 2.87x10^{-3}\, T^{j+1}/P$, where $j+1$ is, for example, 1.147 for helium. [29]

where $\overline{\lambda}$ is the average thermal conductivity of the gas A the area of the plates, ΔT the temperature difference between plates and d the separation distance.

When the mean free path is greater than the separation distance, heat transfer is described by the free-molecule regime. In this case, gas molecules are likely to travel from the hot surface to the cold surface without colliding with other gas molecules, resulting in the heat conduction being dependent on pressure. Heat conduction between two concentric cylinders is given by

$$\dot{q}_{gas} = k_g a_0 P A_i \Delta T., \tag{5}$$

where k is a constant which is given the value of 1.2 for air. P is the pressure of the gas between the cylinders, A_i the area of the inner cylinder and ΔT the temperature difference between the cylinder surfaces, The combined accommodation coefficient is defined as,

$$a_0 = \frac{a_1 a_2}{a_2 + \left(\frac{A_1}{A_2}\right)(1-a_2)a_1}. \tag{6}$$

The combined accommodation coefficient, a_0, is defined in terms of the accommodation coefficients of the inner and outer surfaces, a_1 and a_2, and the inner and outer surface areas, A_1 and A_2. The combined accommodation coefficient is used to make an adjustment for the gas molecules which leave either of the surfaces with a temperature different to that of the surface. Whilst a number of factors affect the value of each surface's accommodation coefficient, a simplification often used in cryogenic designs is $a_1 \approx a_2 \approx 0.5$. This results in the combined accommodation coefficient given by

$$a_0 = \frac{0.5}{1 + \left(\frac{A_1}{A_2}\right)0.5}. \tag{7}$$

2.1.3 Thermal Radiation

Thermal radiation arises from the fact that all objects emit and absorb electromagnetic radiation with a spectrum of intensity as a function of wavelength which is dependent on temperature. This results in a net radiation heat transfer between objects at different temperatures. The Stefan-Boltzmann law, for a blackbody[7] gives the total energy flux density at a particular temperature,

[7] A blackbody is regarded as a perfect emitter, and thus a perfect acceptor of electromagnetic radiation. i.e. ε=1

$$\dot{\mathrm{E}} = \sigma T^4., \tag{8}$$

where σ is the Stefan-Boltzmann constant and T is the absolute temperature.

Generally for all ε,

$$\frac{\dot{q}}{A} = \varepsilon\sigma T^4. \tag{9}$$

In a cryostat thermal radiation becomes significant because of the large difference in temperature between surfaces at operating temperatures and at room temperatures. The net radiation heat transfer, $\dot{q}_{rad}$, where E is a factor dependent on the emissivity's of the hot and cold surfaces, and A is a factor related to area the geometry of the hot and cold surfaces is given by

$$\dot{q}_{rad} = \sigma \mathrm{E} A(T_2^4 - T_1^4), \tag{10}$$

where A is the surface area of the smaller plate. For long coaxial cylinders A is the surface area of the inner surface.

Highly polished metals, films and foils have the lowest emissivities from about 0.01 to 0.1 depending on the type of metal and impurity content[8]. As oxidation on the surface increases, the emissivity also increases, and can be as high as 0.6 for highly oxidised copper. Glass, carbon, paints and varnishes are in the region of 0.8 to 0.9. A guideline for emissivity is if the surface is specular (highly reflective) and lighter in colour, then $\varepsilon \ll 1$,. Alternatively if the surface is diffuse and duller, $\varepsilon \approx 1$. Equations to calculate E for both specular (Equation 11a) and diffuse (Equation 11b) reflection of long coaxial cylinders are given below where A_1 and A_2 is the surface area of the inner and outer cylinder respectively. These equations use the average emissivity of a surface, and do not account for the anisotropy of emissivity in non-ideal materials.

$$\mathrm{E} = \frac{\varepsilon_1 \varepsilon_2}{(\varepsilon_2 + \varepsilon_1 - \varepsilon_1 \varepsilon_2)}, \tag{11a}$$

$$\mathrm{E} = \frac{\varepsilon_1 \varepsilon_2}{[\varepsilon_2 + (A_1/A_2)(\varepsilon_1 - \varepsilon_1 \varepsilon_2)]}, [12]. \tag{11b}$$

[8] Emissivity and electrical resistivity are related by the equation $\varepsilon \equiv 365(\rho/\lambda_r)^{0.5}$ where ρ is the resistivity and λ_r the wavelength of the radiation in micrometers. Since pure metals have a lower resistivity at cryogenic temperatures, it follows that their emissivity is lower. [19]

To reduce radiation heat transfer, either superinsulation or a thermally anchored radiation shield can be installed. Superinsulation is a thin reflective material, and is installed in many layers. The contact between layers of superinsulation should be minimised by either lightly crinkling it, or using spacers to isolate the layers. Alternatively, prefabricated multilayer insulation blankets can be purchased. Equation 12 gives the heat flow when using a superinsulation shield, where N is the number of insulation layers [12],

$$\dot{q}_{MLI\_shield} = \frac{\dot{q}_{rad}}{1+N}. \tag{12}$$

It is also important to consider the pressure of the environment in which the superinsulation shield will be used. As pressure increases, the heat conduction from the gas present increases between the layers of superinsulation and reduces its effectiveness of the shield. Figure 2.1 shows the effect of pressure on apparent thermal conductivity for superinsulation. From this figure it is clear that a pressure below 1 Pa is desirable, and consequently that the vessel needs to remain below this level of vacuum for the superinsulation to remain effective.

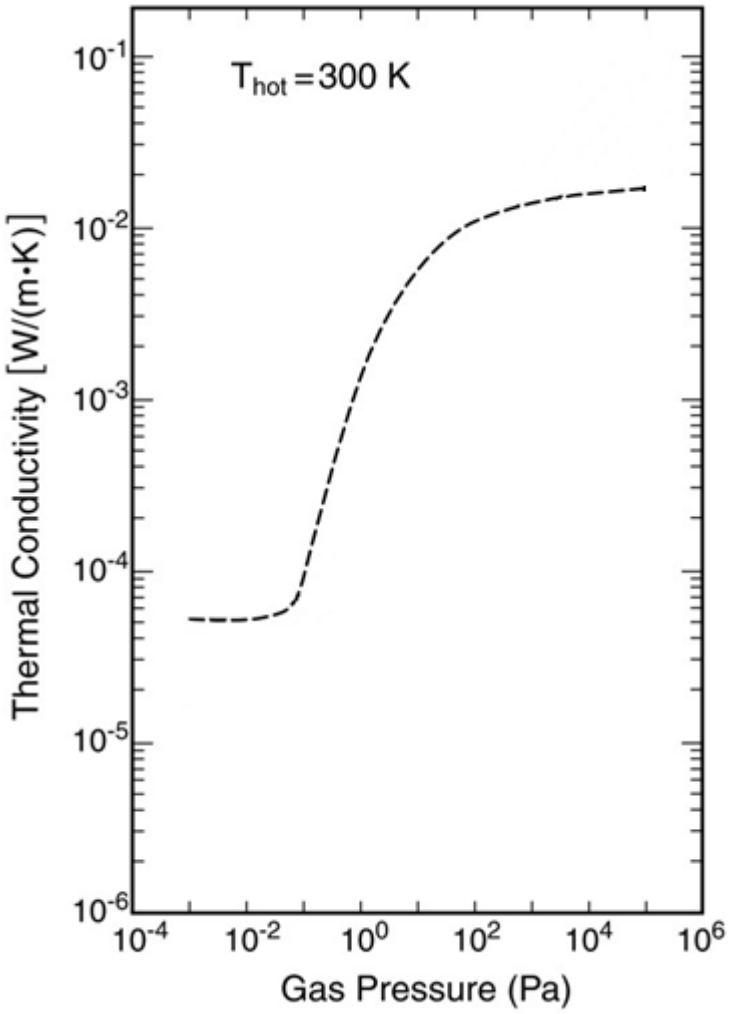

Figure 2.1 Gas Pressure vs. Apparent Thermal Conductivity for 'crinkled' Superinsulation (NRC-2). Hot wall temperature (T_{hot}) is 300 K and cold wall temperature is 79 K. Adapted from [12]

A thermally anchored radiation shield is also very effective in reducing thermal radiation. It is a metallic jacket which surrounds the cold surface (experimental stage) and is cooled by alternative source. Often it is cooled down by liquid nitrogen, but in designs with two-stage cryocoolers it can be thermally anchored to the 1st stage. The approximate reduction of heat when using the shield,

$$\dot{q}_{rad\_shield} = \dot{q}_{rad}\left(\frac{T_{shield}}{T_2}\right)^4 \tag{13}$$

where T_{shield} is the temperature of the radiation shield and T_2 the temperature of the hot surface. This does not account for the emissivity of the shield surfaces. The dependence of the shield temperature can quite clearly be seen. If the shield is connected to the 1st stage of the cryocooler, it is important to remember that the heat flow into this stage increases. Thus it is often beneficial to wrap the shield in superinsulation.

2.2 Cryostat Design Calculations

The cryostat was designed and built around an Scanning Electron Microscope (SEM) vacuum chamber. A 'bucket' experimental stage was constructed with piping to transfer liquid nitrogen, and a radiation shield. The coldhead of the cryocooler was mounted vertically on top of the SEM. Although the focus of this section on is the design of this cryostat, several additional comparison calculations have been done to highlight choices made.

2.2.1 Cryocoolers and Liquid Cryogens

The decision between the use of a cryocooler or a liquid cryogen is that of cost, complexity and flexibility. Liquid cryogens are often readily available, and much of the complexity in their use lies in minimising the heat flow into the cryocooler to lessen boil off of the cryogen. Temperature control of the experimental stage is generally performed by constructing a thermal link between it and the cryogen and using a heater. The flexibility can be increased at the cost of greater design complexity. Appendix Table B. 1 gives the latent heats for vaporisation of several common cryogens. Cryogens have the disadvantage of requiring delivery and storage.

Cryocoolers are reasonably pricey, depending on the cooling power, lower temperature limit and type. They offer the most flexibility as temperature control can be done using a heater. Cooling power is the most limiting factor in their use and the design of the cryostat impacts the attainable temperature.

FCL's which use HTS materials are often cooled with liquid nitrogen due to simplicity in the design. If a liquid cryogen is used for an MgB_2 (T_c = 39 K) based FCL, it would need to be liquid neon, hydrogen or helium. Using a cryocooler becomes economically viable because of the expense of these cryogens, and it is safer when considering using liquid hydrogen.

2.2.2 Cryocooler Cooling Power

The operating temperature of a two-stage cryocooler is determined by considering the heat input in relation to the available cooling power, at each stage of the cold head. The cooling capacity curve for the Cryomech GB15 Cryorefrigerator, which has been used in this work, can be seen in Figure 2.2. By selecting the operating temperature of the second stage, an upper bound for heat input to each stage can be found. Power levels corresponding to the first stage are represented with roughly vertical lines and those corresponding to the second stage have roughly horizontal lines. It is necessary to interpolate the lines to obtain the heat

input values. Using the data from Figure 2.2, the upper bound heat inputs for a second stage temperature can be expressed graphically as shown in Figure 2.3 for 20 K (green line on Figure 2.2).

Conversely, the heat input to each stage of the cold head can be found by measuring the temperatures at each stage when the system is in steady state and any heat sources within the cryostat have been suppressed. This can be used to provide feedback concerning the accuracy of the design.

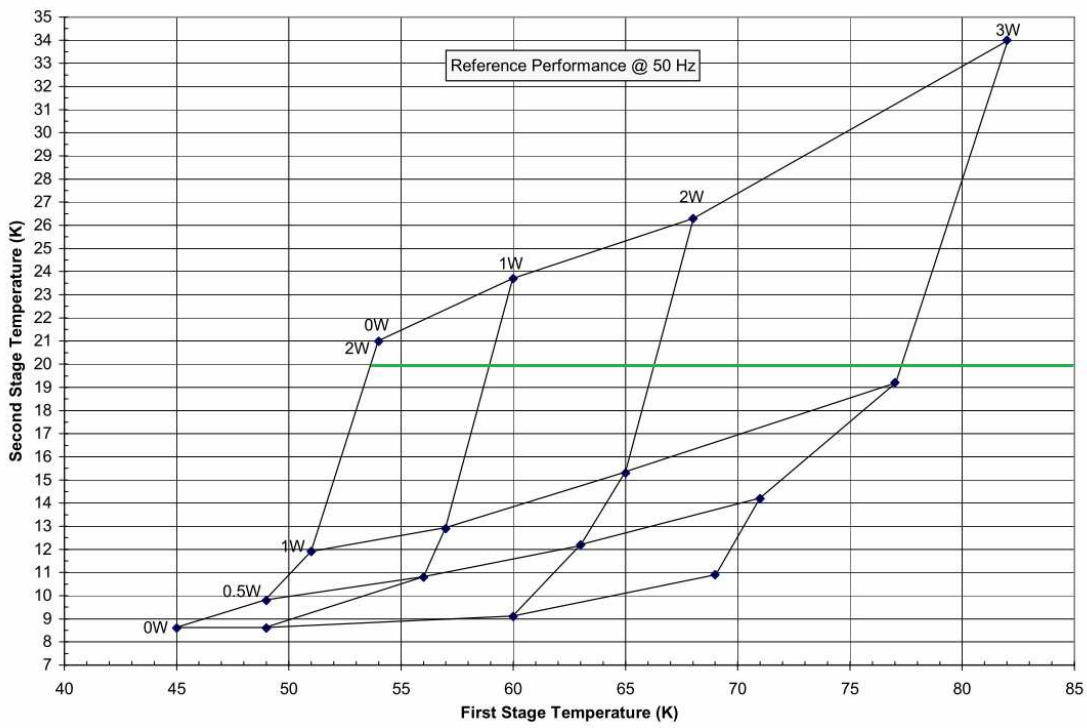

Figure 2.2 GB15 Cryorefrigerator Capacity Curve (when used with a power supply at a frequency of 50 Hz) [36]

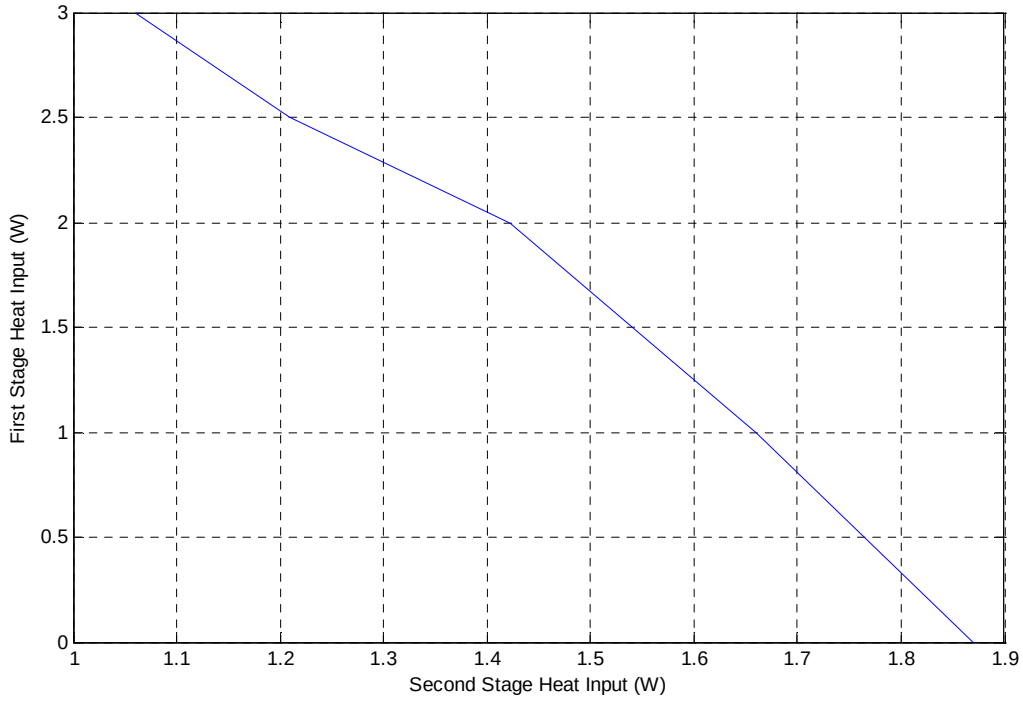

Figure 2.3 Graph of First Stage Heat Input vs. Second Stage Heat Input @ 20K derived from cooling capacity curve

2.2.3 Heat Conduction – Imperfect Vacuum

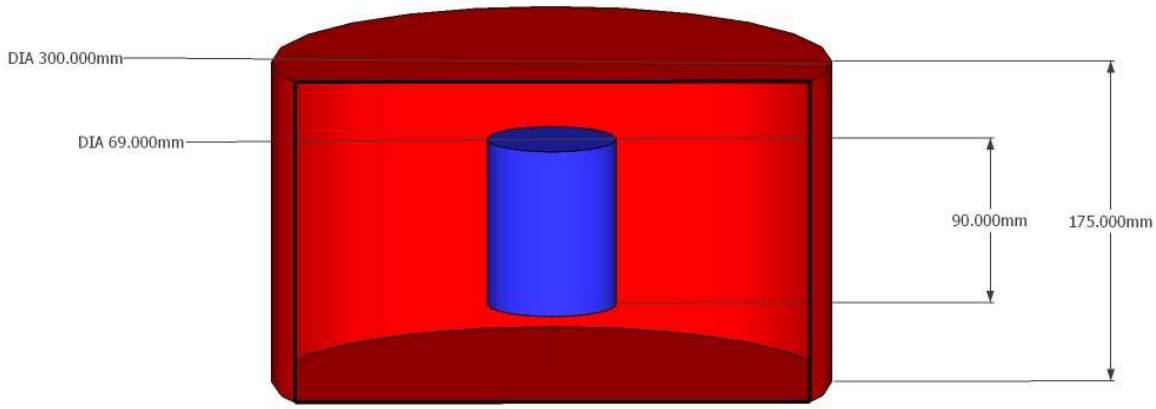

Figure 2.4 Model for Thermal Radiation of the Experimental Stage with hot surface (red) surrounding the cold surface (blue)

Figure 2.4 provides a simplified model of the cryostat inner wall (red), and the experimental 'bucket' stage (blue). The volume or space between the walls of the cryostat and the cold head is evacuated and placed under medium to high vacuum to reduce the heat conducted through the gas that would have otherwise been present. A pressure below 10^{-3} Pa is regarded as vacuum insulation [12]. As the vacuum of the 'SEM cryostat' is not better than this (0.1 Pa), the residual gas molecules present will still conduct a small amount of heat into the cold

head's first and second stage. Assuming the cold head's second stage reaches 25 K, much of the remaining gases are condensed on the cold head, a process known as cryopumping. In these calculations, *k* is given the value 1.2 (for air) [12], although it is likely higher as ratios of helium and hydrogen increase as temperature decreases. Calculating the inner surface area (blue),

$r_1 = 0.06m,$
$h_1 = 0.09m,$
$A_1 = 2\pi r_1 h_1 + 2\pi {r_1}^2 = 0.0226m^2.$

Calculating the outer surface area (red),

$r_2 = 0.1m,$
$h_2 = 0.175m,$
$A_2 = 2\pi r_2 h_2 + 2\pi {r_2}^2 = 0.1728m^2.$

Calculating a_0 using the simplification for cryogenic materials ($a_1 \approx a_2 \approx 0.5$) which was discussed in Section 2.1.2,

$$a_0 = \frac{0.5}{1 + \frac{A_1}{A_2}(0.5)} = 0.4693.$$

The heat flow into the experimental stage due to conduction through gas at a pressure of 0.1Pa,

$$\dot{q}_{gas} = k_g\, a_0\, P\, A_i\, \Delta T = 1.2 \times 0.4693 \times 0.1 \times 0.0226 \times (300 - 25) = 0.350W.$$

If the pressure was improved to a level of vacuum insulation ($1x10^{-3}$ Pa), the heat flow would be,

$$\dot{q}_{gas\_2nd} = k_g\, a_0\, P\, A_i\, \Delta T = 1.2 \times 0.4693 \times 0.001 \times 0.0226 \times (300 - 25) = 3.50mW.$$

Performing a similar calculation for the first stage, assuming it to have an inner area of $0.0094m^3$, be at a minimum temperature of 77K and at a pressure of 0.1Pa, the heat flow would be,

$$\dot{q}_{gas\_1st} = k_g\, a_0\, P\, A_i\, \Delta T = 1.2 \times 0.4867 \times 0.1 \times 0.0094 \times (300 - 77) = 0.122W.$$

These results demonstrate the importance of maintaining a high level of vacuum, preferably at or below vacuum insulation, $1x10^{-3}$ Pa.

2.2.4 Heat Conduction – Wiring

The heat flow into the system due to wiring can be particularly significant if the chosen wire gauge and/or its thermal conductivity is high, or if care is not taken to thermally anchor the wire at intermediate temperatures such as the 1st stage of the cryostat. Applying Fourier's Law to calculate the heat flow for different materials, areas, lengths and temperatures yields the following results:

Table 2 Heat flow comparison for different materials, areas, lengths and temperature [12]

Material	AWG	Diameter (mm)	Length (m)	T_{high} (K)	T_{low} (K)	$\dot{q}_{cond}$ (mW)
ETP Copper	36	0.1270	0.5	300	25	3.6
	30	0.2548	0.5	300	25	14.4
	36	0.1270	1	300	25	1.8
	36	0.1270	0.5	300	77	2.4
	36	0.1270	0.5	77	25	1.2
Phosphor Bronze	36	0.1270	0.5	300	25	0.24
	30	0.2548	0.5	300	25	0.98
	36	0.1270	1	300	25	0.12
	36	0.1270	0.5	300	77	0.22
	36	0.1270	0.5	77	25	0.02

Phosphor bronze wiring has a much lower thermal conductivity than copper but it is much more electrically resistive. It is useful for the voltage measurements of PT100's and for voltage taps on superconductors. If AWG30 ETP copper were used to wire up five PT100's, with a wiring length of 0.5m, upper temperature of 300K and lower temperature of 25K, the heat flow into the cold stage would be 288mW. Using phosphor bronze reduces this to 19.6mW, a large improvement.

Current leads need to have a low electrical resistivity to reduce Joule heating from becoming significant, and so copper is generally used. However, copper has a high thermal conductivity and thus there is a trade-off between Joule heating (wire gauge) and conductive heat flow.

2.2.5 Heat Conduction – Liquid Nitrogen Inlet Pipe

The 'bucket', the experimental stage of this research, requires two pipes connecting it to the body of the cryostat, one as a liquid nitrogen inlet and the other as a gas exhaust. The piping used it 316 grade stainless steel with the following specifications:

Tube Diameter: 6 mm
Tube Thickness: 1 mm
Tube Length: 50.9 mm
Temperature of Bucket: 25 K
Room Temperature: 300 K
Cross-sectional area of tube = 1.5708 x 10^{-5} m^2

Calculating the heat conducted through the pipe if the bucket is at 25 K,

$$\dot{q}_{ss} = \left({}^{A}/_{L}\right)\int_{25K}^{300K}\lambda(T)dT = \left({}^{1.57x10^{-5}}/_{0.0509}\right)\int_{25K}^{300K}\lambda(T)dT = 0.9358\,W.$$

Clearly this is unacceptable as for two pipes this is 1.87W! To reduce the heat flow the pipe is wrapped around the coldhead to increase its length to 210 mm. The heat flow is reduced to 0.2268 W per pipe. Alternatively thinner pipe could be use, or an external extension to the vacuum space to lengthen the tubes even more.

2.2.6 Thermal Radiation

Figure 2.4 provides the thermal model (excluding radiation shield), and assumes heat is radiating between two concentric cylinders, an inner cool surface, and an outer warm surface, where the outer surface is approximated as being the SEM's inner wall. The outer surface is polished stainless steel and will likely have specular emissivity below 0.1, whilst similarly the inner surface is assumed to have a diffusive emissivity of roughly 0.6 as the surface is lightly oxidized copper. Subscripts 1 and 2 correspond to the inner and outer surfaces respectively. The dimensions of the surfaces can be seen in Figure 2.4.

Below are calculations for thermal radiation between hot (red) and cold (blue) surfaces. Included are calculations when a radiation shield at 77 K is used, as well as two examples of using superinsulation.

$$\mathrm{E} = \frac{\varepsilon_1\varepsilon_2}{\left[\varepsilon_2 + \left(\frac{A_1}{A_2}\right)(\varepsilon_1 - \varepsilon_1\varepsilon_2)\right]} = \frac{0.6x0.1}{\left[0.1 + \left(\frac{0.027}{0.1728}\right)(0.6 - 0.6x0.1)\right]} = 0.3255,$$

$$\dot{q}_{rad} = \sigma \mathrm{E} A_1(T_2^4 - T_1^4) = \left[\frac{5.67x10^{-8}W}{(m^2K^4)}\right](0.3255)(0.0270)(300^4 - 25^4) = 4.034W.$$

When a radiation shield is used and the shield is thermally anchored to 77K, the radiative heat flow is,

$$\dot{q}_{rad-shield-77K} = \dot{q}_{rad} \times \left(\frac{77}{300}\right)^4 = 17.5mW.$$

If 20 layers of superinsulation are used instead of the thermally anchored radiation shield, radiative heat flow would then be,

$$\dot{q}_{rad-superinsulation\,(20\,layers)} = \dot{q}_{rad} \times \left(\frac{1}{N+1}\right) = 192.1mW.$$

Increasing the number of layers of the superinsulation shield would give a radiative heat flow of,

$$\dot{q}_{rad-superinsulation\,(80\,layers)} = \dot{q}_{rad} \times \left(\frac{1}{N+1}\right) = 49.8mW.$$

These calculations highlight the importance of using radiation shielding which is ideally a copper radiation shield thermally anchored to the second stage, or thermally linked to a liquid nitrogen reservoir.

2.2.7 Summery

Summing the heat flow into the first and section stage of the cryostat assuming the second stage reaches 25K and that room temperature is 300K gives the following results:

Table 3 Summery of Heat Flow Calculations

Stage	Type	Source/Details	Heat Flow (W)
1	Conduction	Thermometry, 20x AWG36 phosphor bronze, 0.5m	0.0044
		Current leads, 2x ETP Copper, AWG30, 0.5m	0.0189
		Imperfect Vacuum @ 0.1Pa	0.1224
	Radiation	No shielding	1.0525
	Total:		1.198
2	Conduction	Thermometry, 20x AWG36 phosphor bronze, 0.5m	0.0004
		Current leads, 2x ETP Copper, AWG30, 0.5m	0.0099
		Imperfect Vacuum @ 0.1Pa	0.350
		Liquid nitrogen inlet & exhaust pipes	0.4536
	Radiation	Using 20 layers superinsulation	0.1921
	Total:		1.006

2.3 Cryostat Construction and Testing

A block diagram of the cryostat can be seen below in Figure 2.5.

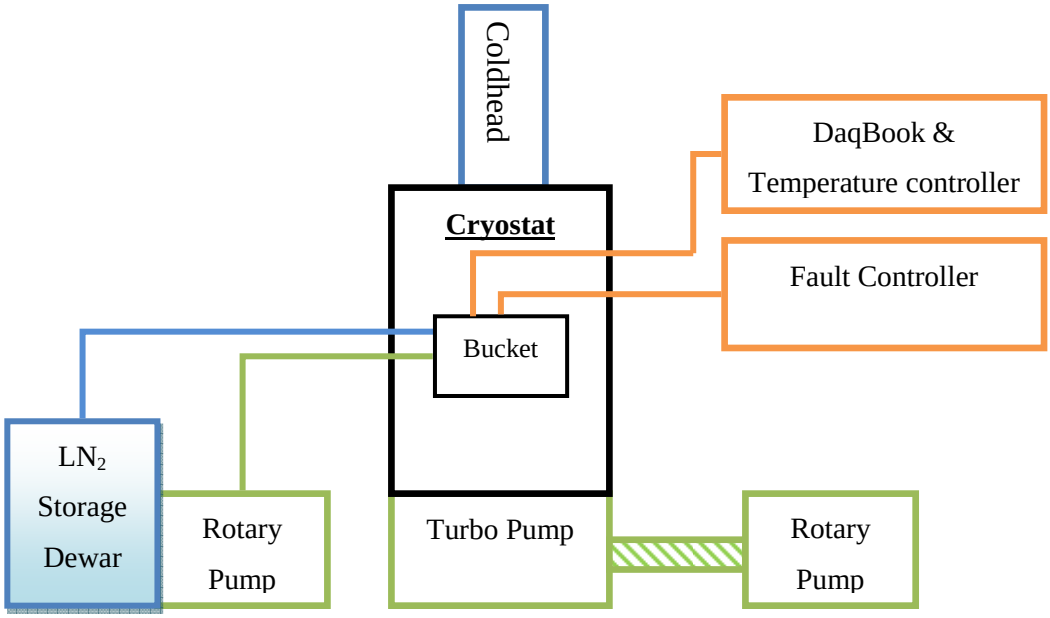

Figure 2.5 Cryostat Block Diagram

2.3.1 Vacuum Chamber

A Scanning Electron Microscope (SEM) vacuum chamber was used as the body of the cryostat. It has numerous electrical lead-throughs, viewports, mechanical access, maintains reasonable vacuum and the chamber is large enough for the experimental stage. Several modifications were made to the vacuum chamber so that it could be used in conjunction with the crycooler's coldhead, EXT75DX turbomolecular pump and pirani gauge. The cryostat can be seen in Figure 2.6, with the underside in Figure 2.7.

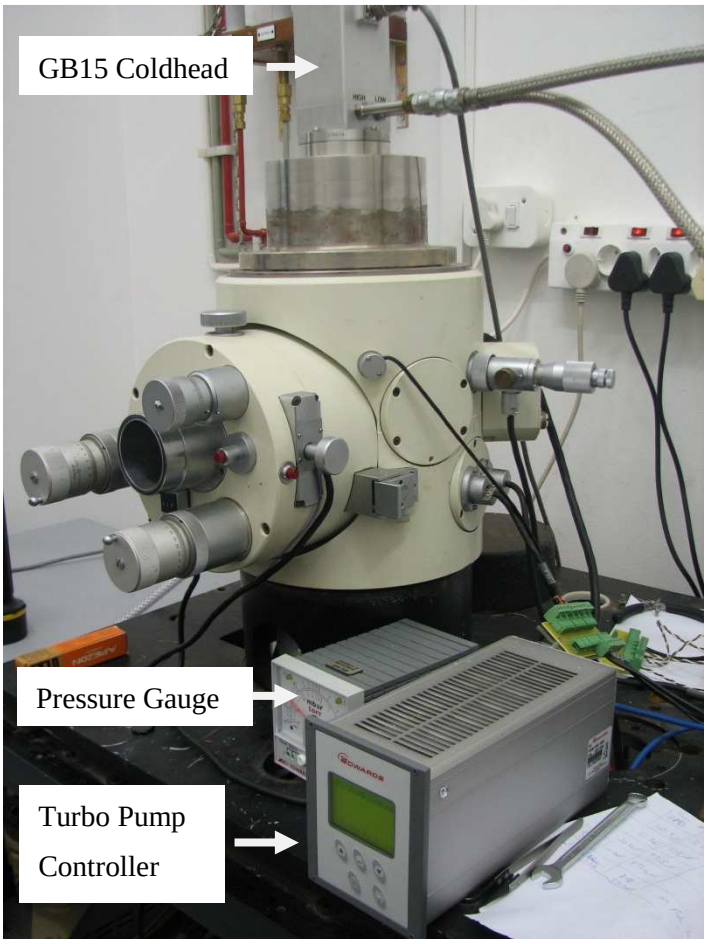

Figure 2.6 Modified SEM vacuum chamber, showing Coldhead, Turbo pump controller and pressure gauge

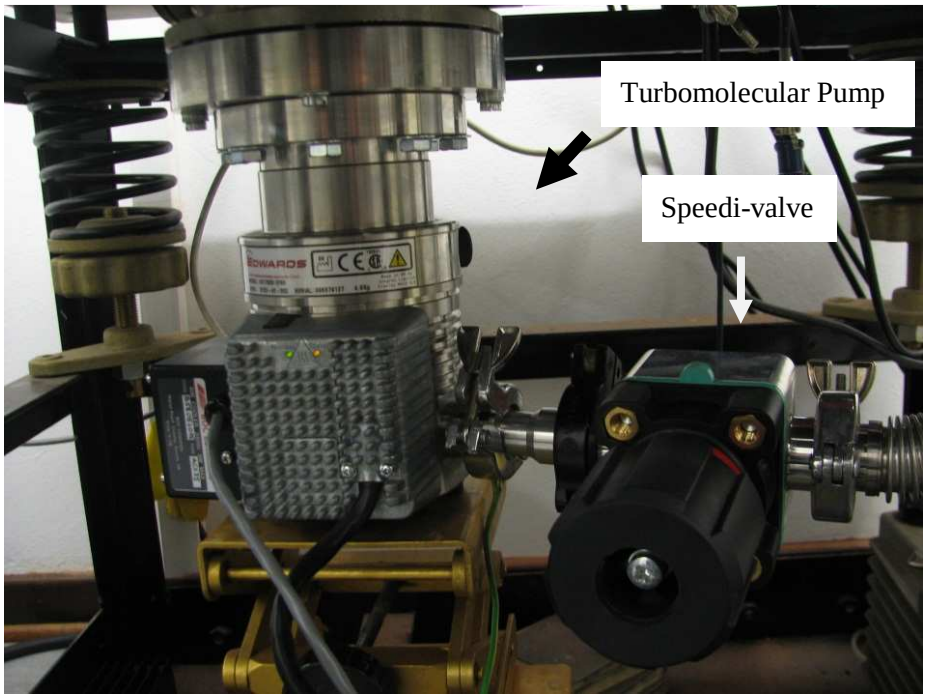

Figure 2.7 Underside of modified SEM vacuum chamber showing turbo pump attachment, turbomolecular pump and Speedi-valve which connects to a rotary pump

The choice of the SEM vacuum chamber was useful because it could be used almost immediately. The level of vacuum was high enough to effectively use the superinsulation and gave a fair vacuum. One problem with selecting the SEM chamber was that working inside the vacuum chamber was particularly difficult due to lack of space, and it was difficult to install the wiring and superinsulation.

2.3.2 Materials Selection

The choice of materials for different regions of the cryostat is important and is governed by properties such as thermal conductivity, specific heat capacity, thermal contraction, and yield strength.

The cryostat's body is generally made from stainless steel or aluminium dependant on weight and yield strength. The grade of stainless steel should be one averse to corrosion such as 316, especially for flanges (as shown in Figure 2.8) which need to be kept clean and smooth to ensure vacuum sealing.

Connections to the coldfinger of a cryocooler are made with copper because of its high thermal conductivity, preferably 99.999% pure annealed copper. Although high purity copper has the highest thermal conductivity for copper alloys, it has proved difficult to source and expensive. A more readily available alloy for wires and small bars with similar

thermal conductivity is either electrolytic tough pitch (ETP) or oxygen free high conductivity (OFHC) copper. Phosphor deoxidised (PD) copper was used for the bucket because of the buckets size, whilst ETP was used for the copper braid thermal link. At 30K, the thermal conductivity of ETP and OFHC is an order of magnitude greater than that of phosphor deoxidised copper.

Brass screws were used to fasten the thermal braid disk (shown in Figure 2.13) to the coldfinger because upon cooling the brass will contract more than the copper and increases the pressure of the join. If stainless steel screws were used, the copper would contract more and the pressure would be reduced. This is a good example of how the selection of materials with certain thermal contraction coefficients can improve the design of the cryostat. Alternatively if it is ignored and the thermal contraction of the screws is much less than the bucket material, the two pieces could pull apart.

2.3.3 Temporary Vacuum Seals

The majority of temporary vacuum seals were at room temperature and made using Nitrile Rubber O-rings with a light coating of vacuum grease. They are reliable, inexpensive and can be replaced quite easily. Additionally they are easy to source. In medium to high vacuum systems, o-rings and the flanges which they are in contact with must be kept particularly clean so that the integrity of the vacuum is insured. They are not used in ultrahigh vacuum systems.

Temporary seals for use at cryogenic temperatures are slightly more difficult to design. Rubber (O-ring) seals cannot be used as they become brittle at low temperatures [12]. The alternative is to use metal seals such as pure indium wire rings, C-rings, or ConFlat™ flanges (with copper gaskets).

The ConFlat™ flange seal consists of two flanges and a copper gasket which is shown in Figure 2.8. The flanges have a ‘knife-edge’ which, when bolted down, cuts into the copper gasket providing a very good seal. It can be used down to pressures between $10^{-5} - 10^{-11}$ Pa depending on seal manufacturer, quality of the copper gasket, cleanliness of mating surfaces and backout preparation. It is best to follow the manufacturer’s torque rating for the bolts - which is dependent on the size of the flange - and ensuring the bolts used are capable of achieving this. There was one temporary cryogenic seal made in the design, namely, the wiring insert for the copper bucket. It was made using the ConFlat™ flange seal.

Figure 2.8 ConFlat™ Flanges and Copper Gasket [37]

2.3.4 Cryogenic Electrical Lead-through

Electrical lead-throughs capable of withstanding cryogenic temperatures are more difficult to manufacture than standard lead-throughs because the difference in thermal contraction of different materials. The method presented below in Figure 2.9 uses epoxy, brass or stainless steel tubing, and some heat-shrink[9]. The heat-shrink is shrunk around the higher pressure side of the join and is filled with epoxy (Stycast or similarly filled epoxy is recommended to better match the thermal contraction of the tube). Epoxy's thermal contraction is greater than that of the tube, and so upon cooling it shrinks onto the tube. If the 'lip' is not given using the heat-shrink, the epoxy will contract and pull away from the tube, breaking the vacuum seal.

[9] A sleeve made of nylon which permanently shrinks in diameter upon heating

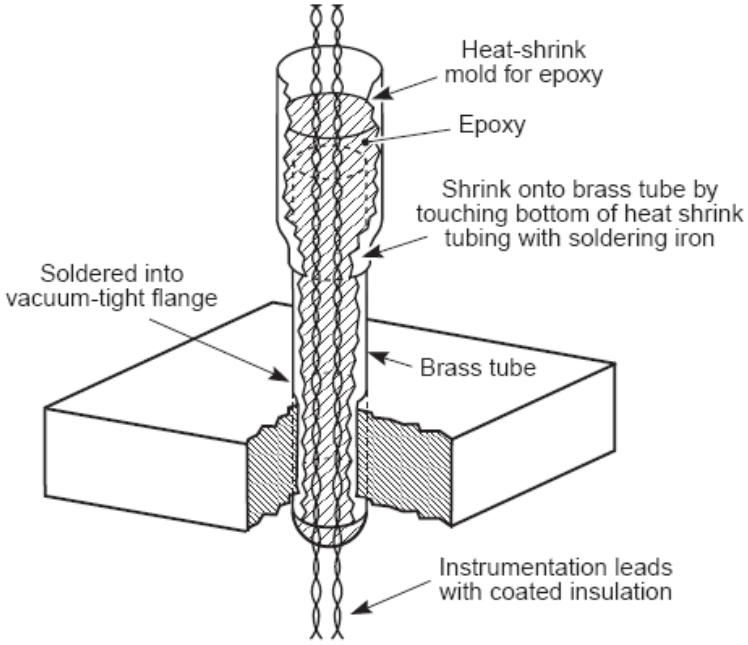

Figure 2.9 Cryogenic Electrical Lead-through [12]

2.3.5 Experimental Stage

The copper bucket which housed the probe and solid nitrogen is the expermental stage of the croyostat and is shown below in Figure 2.10. The seal for the top flange needs to work at cryogenic temperatures and so a Conflat flange was used with a copper gasket seal, as dicussed above. The bucket assembly with a pair of inlet pipes can be seen in Figure 2.10 and in Figure 2.11. The pipes allow the liquid nitrogen to be pumped into the bucket.

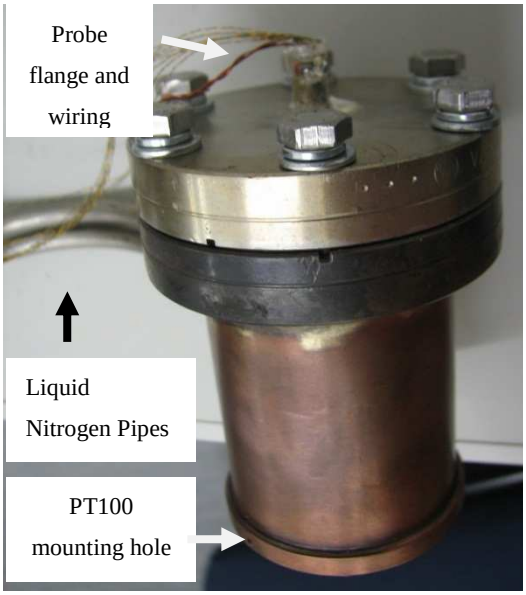

Figure 2.10 Experimental Stage showing copper bucket, liquid nitrogen pipes, flange and wiring

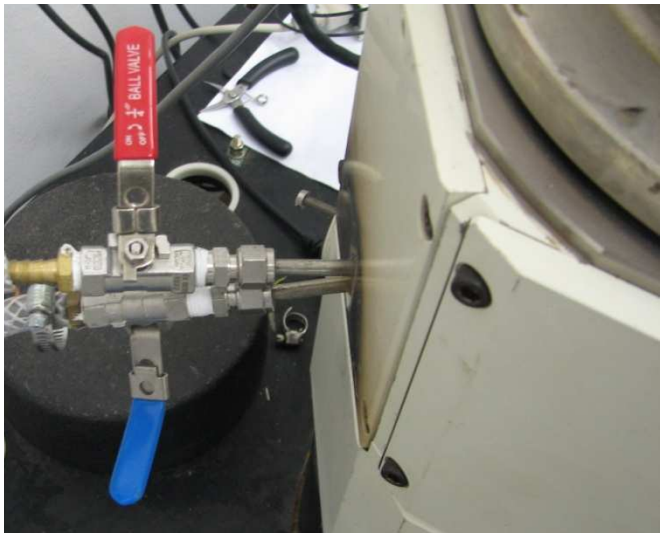

Figure 2.11 Experimental Stage Piping

2.3.6 Coldfinger Thermal Link to Experimental Stage

The thermal link between the coldfinger and the base of the copper bucket is a flexible copper braid. Using the flexible braid allows it to be soldered to the bucket base and to a disc which can be fastened to the coldhead. If a solid bar is used, it is not possible to fit it through the opening in the cryostat.

The copper braid is a second revision of the thermal link. The original thermal link was an ETP copper bar which was clamped to the bucket and fastened to the coldhead using M3 screws, as shown in Figure 2.12. The reason for abandoning the copper conduction bar was the difficulty ensuring the bucket and conduction bar were both perfectly horizontal. Perfect alignment of the bar-bucket join would maximise the join's surface area. In this case, the misalignment of the bar-bucket join caused the thermal contact resistance across it to be variable/unreliable and higher than desired. It was one of several corrected factors that prevented the bucket reaching the designed temperature during initial testing.

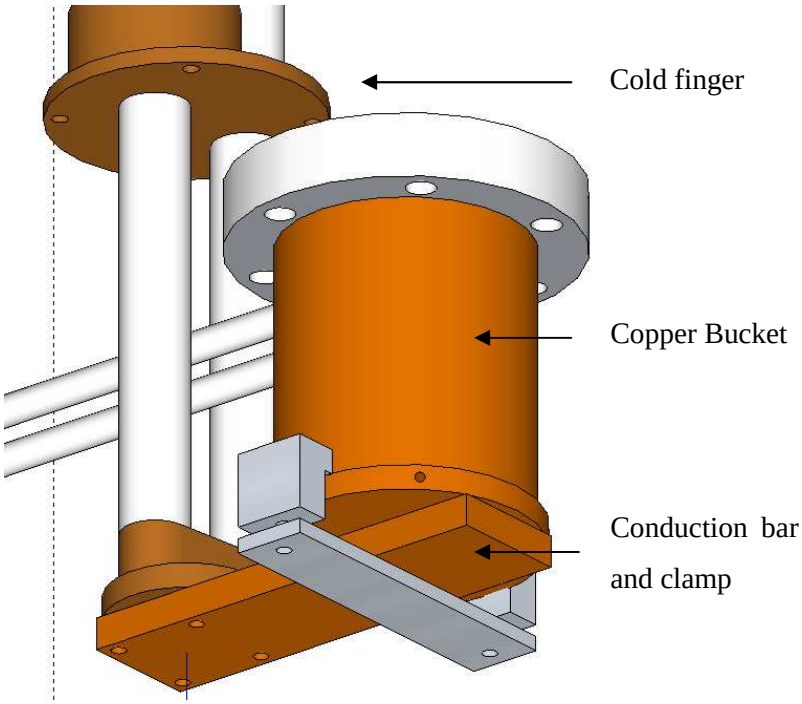

Figure 2.12 3D Rendering of Copper Bucket with Conduction Bar (not braided link)

The final version of the experimental stage base can be seen in Figure 2.13. Nichrome heater wire was wrapped around the lower section of the copper bucket and used to control the temperature of the experimental stage. It is positioned close to the PT100 which is mouted in the hole on the bucket 'lip'.

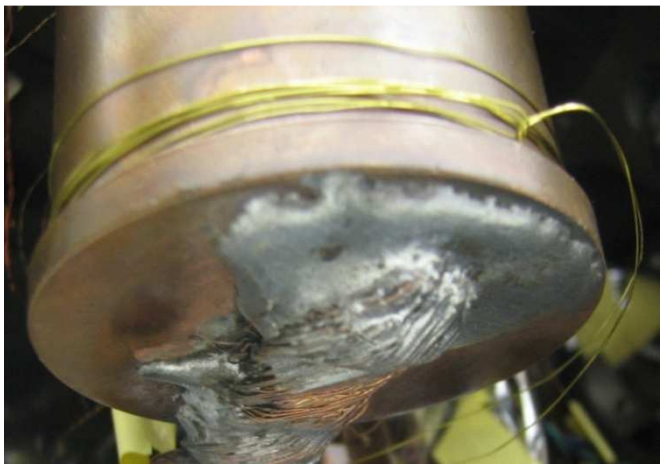

Figure 2.13 Final Experimental Stage Base showing soldered copper braid and nichrome heater

2.3.7 Ultimate Pressure

Using a turbomolecular pump (Edwards EXT75DX) with a rotary backing pump the vessel reached an ultimate pressure of 0.1Pa, which is low enough for the superinsulation's apparent thermal conductivity to be minimal (see section 2.1.3).

2.3.8 Radiation Shield (Experimental Stage)

Superinsulation was used for the bucket's radiation shield; 20 layers were wrapped on the inside of a partial cube made from copper sheeting and fitted around the bucket. The superinsulation was held fastened to the cube using cryogenic tape. Initially only 4 sides of the shield were installed because of the difficulty installing a full shield inside the SEM, but this proved to be inadequate with the temperature only reaching 82 K. Adding a top to the shield and wrapping part of the coldhead up in superinsulation improved the situation significantly and allowed the bucket to reach 40 K. The shield can be seen in Figure 2.14.

Figure 2.14 Superinsulation Radiation Shield with copper former

2.3.9 Unloaded 2nd Stage Temperature

The second stage was cooled to its unloaded (no experimental stage) temperature several times, with differing levels of shielding. This serves as a useful comparison to illustrate the benefit of adding in a copper radiation shield anchored to the 1st stage of the coldhead including superinsulation on the outside of the copper shield. The addition of the copper shield without using superinsulation resulted in an increase in ultimate temperature. The likely reason for this is that the additional heat input into the first stage, due to the size and shape of the copper shield, which limits the 2nd stage temperature (see the GB-15 cooling capacity curve, Figure 2.2). The ultimate unloaded second stage temperature with this cryostat was measured to be 12.37 K when superinsulation was added to the outside of the copper shield. This can be further improved by adding superinsulation to the inside of the copper shield. The comparison graph can be seen in Figure 2.2.

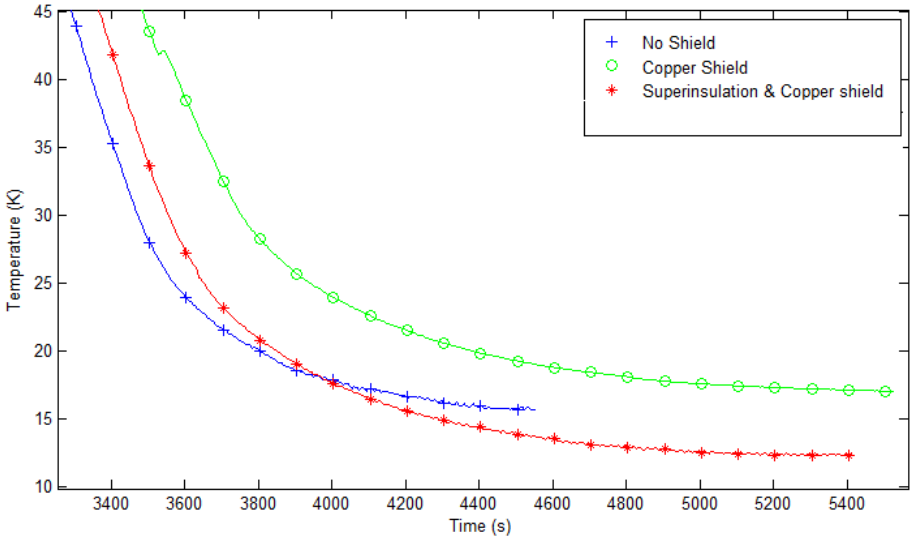

Figure 2.2 Graph of Temperature vs. Time for different levels of shielding

2.3.10 Verification of Nitrogen Solidification

Once the cryostat was assembled, a test was carried out to ensure that liquid nitrogen could be solidified. After placing the SEM chamber under vacuum, the bucket was pre-cooled with liquid nitrogen and the cryocooler turned on. Once the cryocooler started to maintain a temperature below 77K, the bucket was filled and the temperature of the bucket monitored. Figure 2.15 shows the bucket temperature during this period and the gradient change in the region of 63K is indicative of the solidification process taking place.

Cooling further shows the alpha-beta phase change taking place, see Figure 2.16. At this point the temperature inside the bucket is lagging the actual bucket temperature. The bucket ultimately reached 30K, however this is without the probe wiring flange. The bucket temperature reached 40 K when using the probe wiring flange.

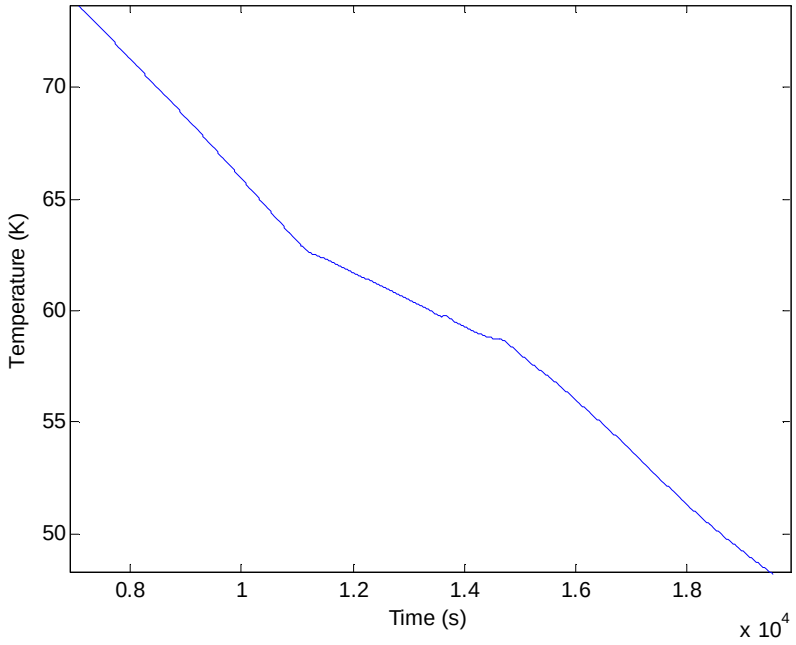

Figure 2.15 Temp versus Time showing liquid nitrogen solidifying 63.15 K

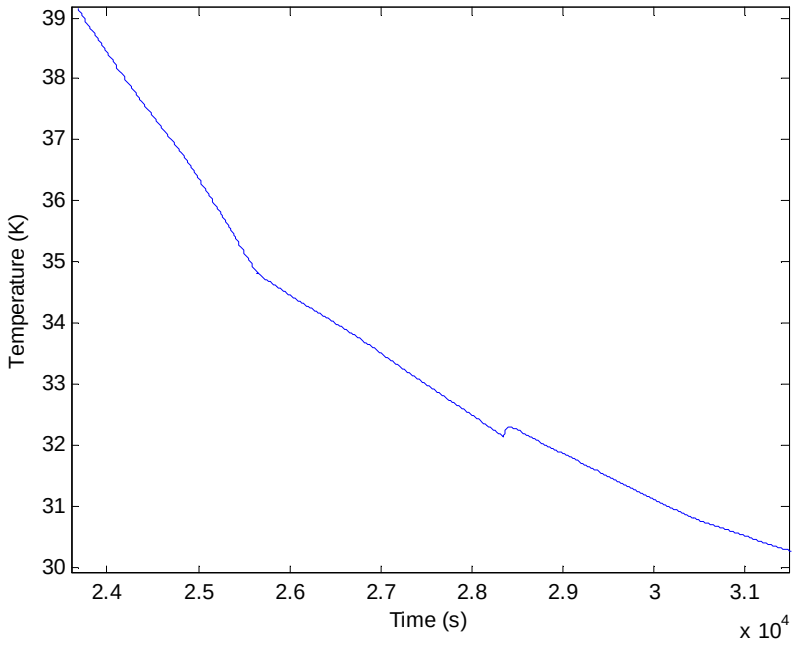

Figure 2.16 Temp versus Time showing the alpha-beta phase change (35.6 K) which is observed at 34.5 K as the temperature of the bucket is lagging the sensor

2.4 Surge Current Equipment

The surge current equipment is used to create high current pulses of variable pulse length. The pulses are used to create the transient heating conditions to test the performance of the thermal battery. It can also be used to test the critical current of a superconductor.

2.4.1 Electronics and Control

The circuit diagram of the pulse equipment can be seen in Figure 2.17. A variac is used to control the voltage across the step down transformer (ratio 14:1) which in turn sets a voltage across the "SFCL" resistor. The "SFCL" resistor is used to simulate the normal state of a superconductor. It allows for pulse powers of up to 50 W_{RMS}. The Desktop Tester Power Control connection (P11) is used to energize the main variac core prior to the "fault" occuring. The Desktop Tester Output plug connects to the an electrical feedthrough socket on the cryostat.

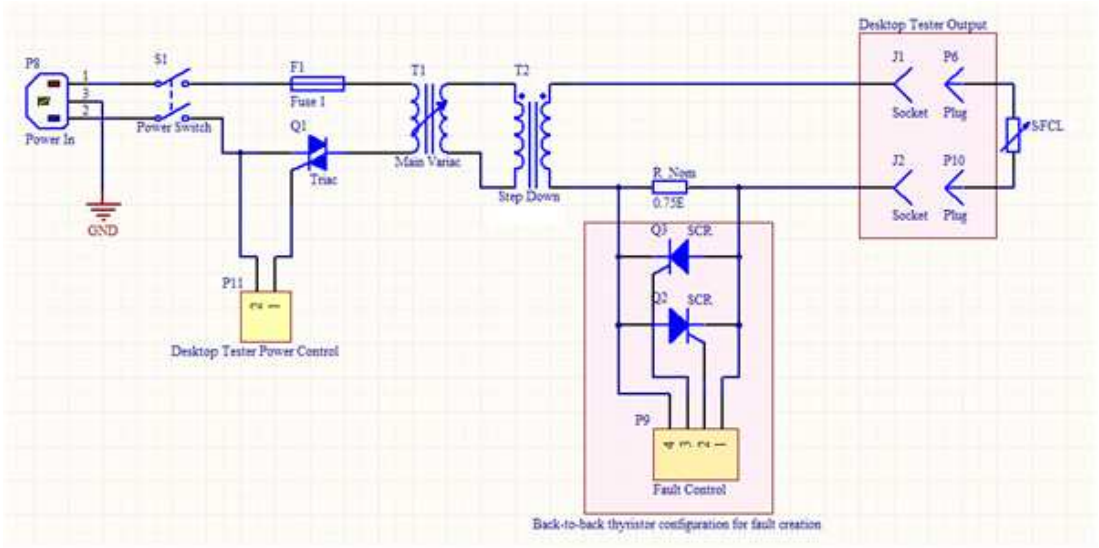

Figure 2.17, Desktop Tester Pulse Equipment Circuit Diagram [38]

The Power Control and Fault Control circuitry is triggered by the Fault Controller Module seen in Figure 2.18 [38]. This module allows fault pulses to be configured with a duration from 50ms to 12s. The firmware can easily be updated to allow for longer pulse durations and repeatitive pulsing occuring at an interval which can be set. The solid state relay's used were Siemens 3RF2350-3AA02 and trigger at zero crossings.

The Daqbook seen in Figure 2.18 is used for temperature measurement and to sample the triggering of the Fault Control circuit. Shielded coaxial cabling is used to connect the Daqbook to measurements to reduce interferance. The voltage signals being sampled across each PT100 are small. At 30 K they have a resistance in the region of 3 Ω. At this

temperature the sensitivity of the PT100 is 0.195 Ω/K. If the excitation current is 1 mA and there is 50 uV of noise, the temperature will vary by 0.25K.

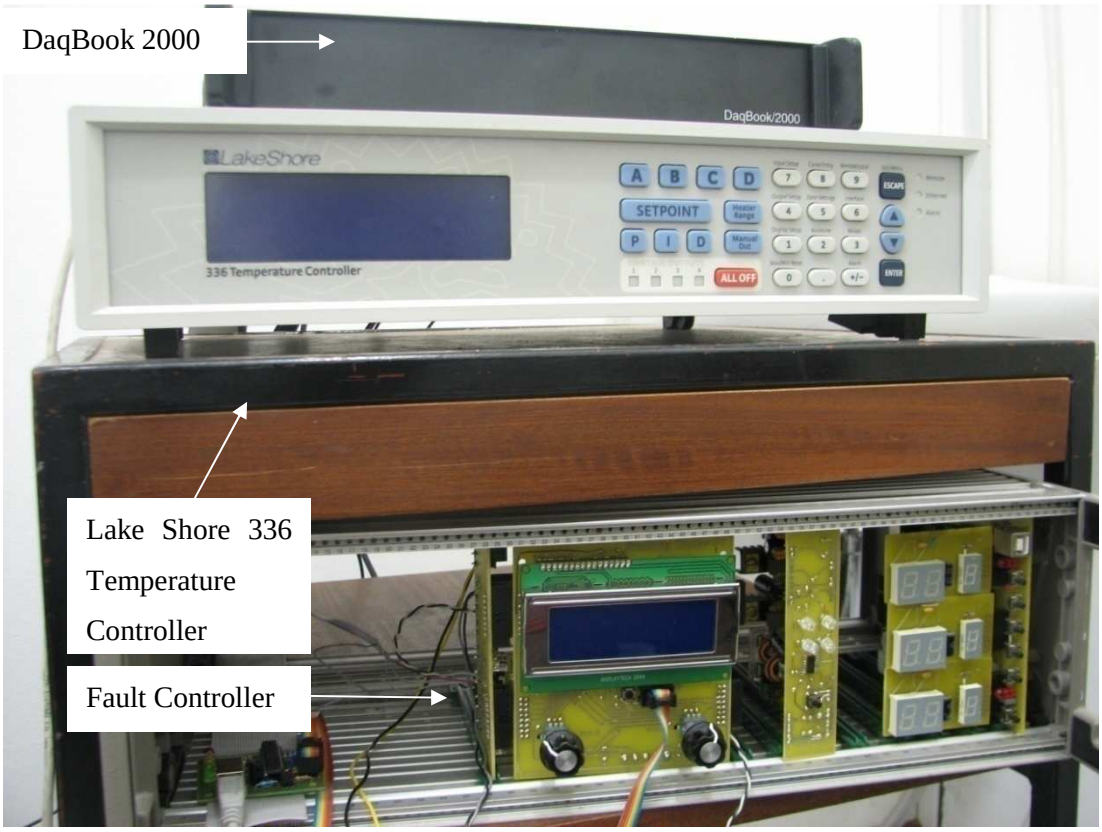

Figure 2.18 Fault Controller Module, DaqBook 2000 and Lake Shore 336 Temperature Controller

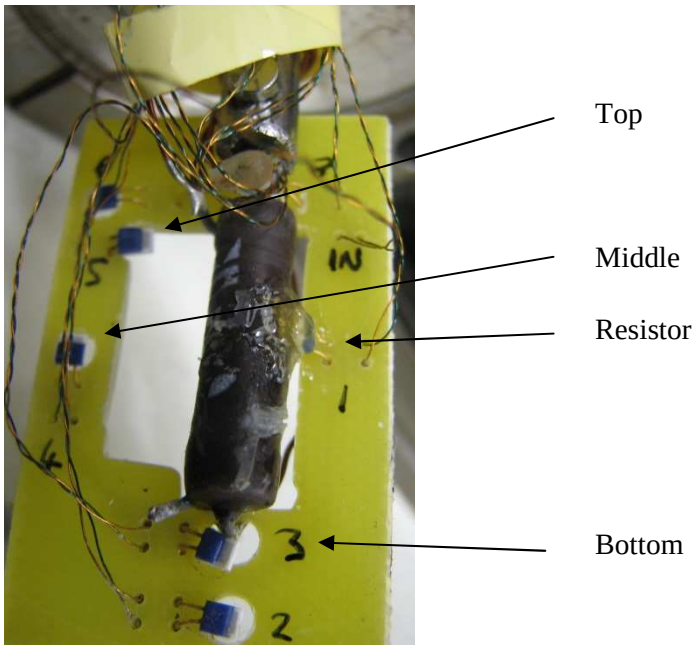

Figure 2.19 Pulse Resistor and Thermometer Array

The wiring and measurement probe shown in Figure 2.19 used for the experimentation is based upon a Conflat flange and comprises of the pulse resistor and thermometer array. It fits into the top of the copper bucket. A resistor is used in place of a superconductor to simulate a superconductor's normal state. It is bolted into the top of the copper bucket as shown in Figure 2.10. A 4.8 Ω 3W metal film resistor was used. Metal film technology was chosen due to its low temperature coefficient (±5 to ±50 ppm/K [39]). Although this would not have been tested at cryogenic temperatures it appeared stable when testing prior to experimentation.

2.4.1.1 Thermometer Array

Thin film PT100's were chosen for the thermometer array because of their low cost, high reproducibility and small time constants. Their sensitivity is less at lower temperatures as shown in Figure 2.20[12].

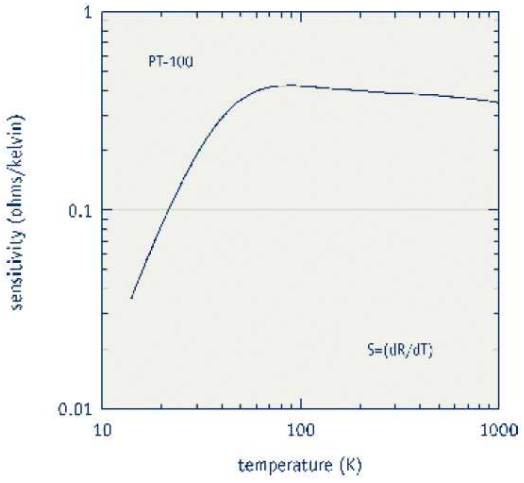

Figure 2.20 Temperature vs. Sensitivity for PT-100 [40]

Thermometers 1, 3, 4 and 5 (seen in Figure 2.19) were used for experimentation. The other 3 were not used as wiring was damaged at the flange input and the solution would be to rewire the entire probe. These thermometers were purchased uncalibrated and rough calibration was done using its resistance at liquid nitrogen temperatures and adjusting the temperature vs. resistance reference curve. The numbering of the thermometers in Figure 2.19 corresponds to the numbering of thermometers shown in subsequent graphs.

Thermometers are connected in series to allow them to be driven by a single current source and measurements of the voltage are done differentially. The current source used is a Lakeshore 120 Current Source.

2.4.1.2 PT100 Thermal Response Time

The thermal response time of a PT100 is dependent on the heat capacity of the sensor; i.e. on the product of the weight of the sensor and the specific heat capacity of the material it is made from. Since specific heat capacity decreases as a function of temperature, the thermal response time also reduces with temperature.

The nature of the thermal disturbance measurements to be carried out requires that the response time of the temperature sensor be small, and hence the requirement for a small heat capacity. Thin-film PT100 sensors are adequate for this application at low temperatures.

The thermal response time for a Thin-film PT100 was measured experimentally by subjecting the sensor to transient thermal conditions. The temperature transient was varied from a few degrees to tens of degrees and averaged to produce the results shown in Table 4. The response times shown in this table are useful to consider when performing transient heating measurements at 60 K, although the response times will improve when performing measurements at lower temperatures.

Table 4, Table of Thermal Response Times for PT100 Sensors

Temperature	**300 K**	**77 K**
Lakeshore PT-111 [40]	20 s	2.5 s
RS Thin-film PT100 (362-9840)	3 s	11-20 ms

2.5 Software

2.5.1 Interface to Temperature Controller

A Lakeshore 336 Temperature Controller has 4 thermometer inputs, a 50 W output and a 100 W output. It has PID control for the outputs with auto tuning functionality and temperature zoning to adjust PID parameters in different temperature ranges. The device can be accessed via its RS232 interface or over Ethernet. The sampling rate on each input is 10Hz.

The software written to access and control the controller makes use of its Ethernet interface and interface commands. The TCP/IP connectivity and many of the useful commands were compiled into a Dynamic-Link Library (DLL) to be easily distributed and used across different application. Features implemented include temperature measurement, set point, output ramping, output control/ranging and temperature zoning.

Software applications written for the Temperature Controller include: Temperature Logging, Temperature Control and Curve Entry/Modification.

2.5.2 DaqBook Measurement Logging

The IOTech DaqBook 2001, a computer data acquisition device shown in Figure 2.18, was used to log the temperature data from the thermometer array. It has analogue inputs and Digital I/O with a maximum sampling rate of 200 kHz across 16 channels. The analogue inputs can be configured differentially which is beneficial to the PT100 resistance measurements. DASYLab, a data acquisition software package, was used to perform some basic processing and log the data. Resistance measurements are logged as well as the calculated temperature values.

2.5.3 Data Processing

Although all cabling external to the cryostat was shielded, there was still ±500 μV_{RMS} of noise present on the measurements, which corresponds to a temperature variation of ±0.1K at 60K. The data was filtered with an 8^{th} order Bessel Filter at 150 rad/s which was designed and run using Simulink in MATLAB. The bode plot for the filter can be seen in Figure 2.21.

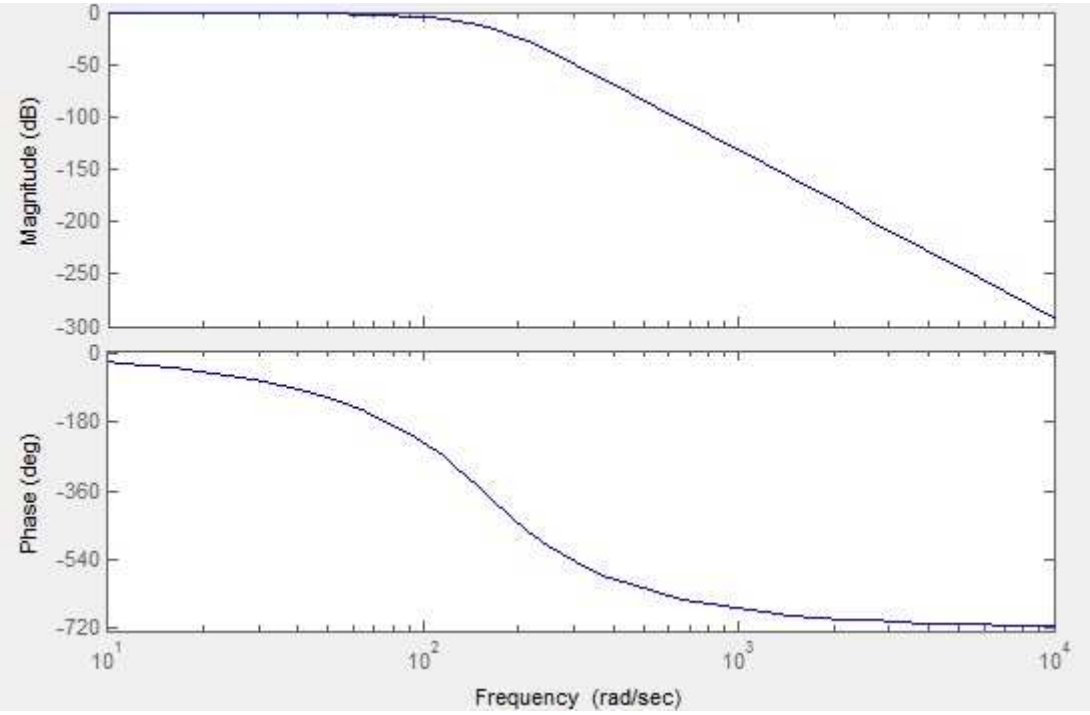

Figure 2.21 Bode Plot for 8th order Bessel Filter

2.6 Chapter Conclusions

Considering the relevant mechanisms of heat transfer shows that this subject matter must be dealt with in meticulous detail when constrained by the cooling power of a cryocooler. The theoretical design was implemented and test. Testing results clearly show the improvement of including radiation shielding, especially with a large experimental stage. This was seen with a remarkable temperature improvement of 42 K when using the 'bucket' experimental stage.

The 'bucket' stage was used to successfully solidify liquid nitrogen, and the alpha-beta phase change was seen to occur as well. The cryostat was then prepared for the testing of thermal batteries, and found to be capable of reaching 40 K when using the wiring probe. If a lower temperature is needed, a cryocooler with greater cooling power should be considered.

3 Experimentation and Procedures

Various experiments are needed to assess the performance of the thermal battery. Metrics used for comparison include the recovery time and change in temperature of the resistor. Both are important for SFCL's and highlight the effectiveness of the thermal battery. It is desirable that both of these are small. The change in temperature of a superconductor is important to keep low during quench due to damage which can be caused through thermal stresses and thermal cycling. Recovery time has quality of service implications, as it is not desirable for an FCL to take long periods of time to recover.

3.1 Filling the Bucket with Liquid Nitrogen

Filling the bucket is done using the inlet pipe system. Figure 3.1 shows this system but omitting the ball valves connected to each of the pipes which can be seen in Figure 2.11. The upper inlet pipe is connected to a liquid nitrogen dewar using a section of PVC piping. The lower pipe is connected to a rotary pump using PVC piping and a section of copper piping used as a heat exchanger so that the rotary pump is not damaged. Controlling the pumping rate of the rotary pump using the ball values allow the rate at which the liquid nitrogen is pumped through into the bucket to be adjusted. The bucket can also be placed under vacuum prior to the filling of liquid nitrogen.

As it is difficult to measure how full the bucket is, it should be pre-cooled to 70 K before filling. Once the filling process begins, the quantity of liquid nitrogen in the supply dewar is visually monitored. The volume of the bucket is 71 ml, and it is regarded as being full once the dewar's volume is reduced by 400 or 500 ml. It is difficult to use the outlet pipe as an indicator of the bucket being full. The pipe quickly frosts up and the liquid nitrogen has generally evaporated by this stage.

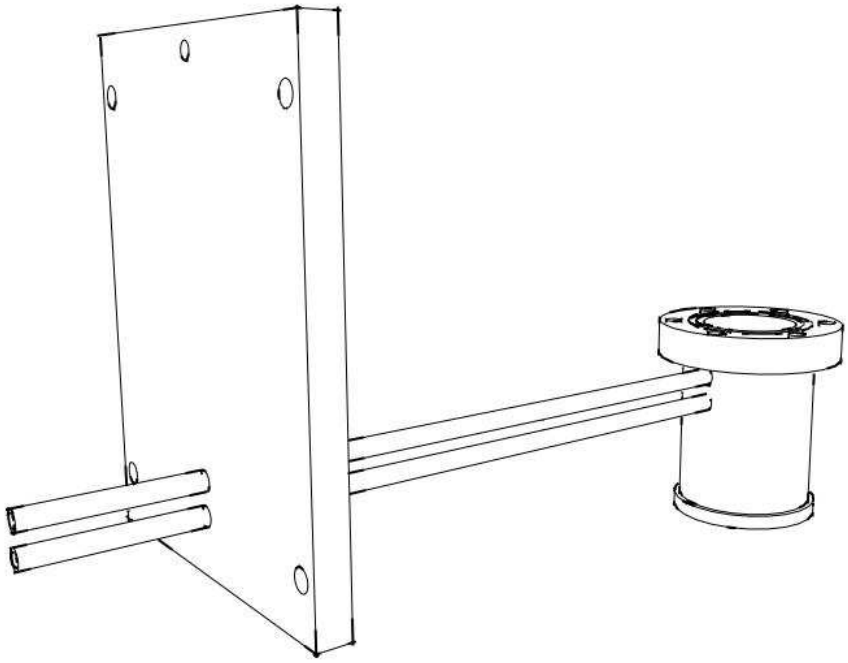

Figure 3.1 Liquid Nitrogen Inlet Pipe System Sketch (not showing bend in pipe)

3.2 Solid Nitrogen Formation Procedure

Temperatures in this section refer to measurements taken from the experimental stage base using a Lake Shore PT-111 (a small PT100) which is used in conjunction with the Lake Shore Temperature Controller. Its original PID settings are adjusted once liquid nitrogen has been added to account for the change in thermal load.

3.2.1 Slowly Formed SN_2 (Cryocooler)

To form solid nitrogen slowly, the cryocooler is used and the cooling rate is controlled. The Lake Shore Temperature Controller's ramping function is used to control the cooling rate to 0.1 K/min. The following procedure is used to form the solid nitrogen slowly:

i. Pump down vacuum chamber pressure to at least 0.1 Pa using turbomolecular pump
ii. Pump liquid nitrogen into the bucket to pre-cool it to 77 K, the boiling point of liquid nitrogen
iii. Turn on cryocooler
iv. Set the Lakeshore PI controller's setpoint to 70 K
v. Pump slowly on the liquid nitrogen in the bucket to evaporate it. This ensures the bucket is empty
vi. Once the cryocooler is maintaining a temperature of 70 K, re-fill the bucket with liquid nitrogen as outlined in Section 3.1
vii. Wait until the temperature is being maintained at 70K once more
viii. Set the PI controller's setpoint to 60K with a ramp of 0.1K/min. At 63.15 K the nitrogen will start to solidify

ix. Once 60 K has been reached experimentation can begin

3.2.2 Rapidly Formed SN_2 (Vacuum)

Pumping on liquid nitrogen is generally used to control the temperature of the liquid, but can also be used to quickly solidify it. The experimentation must be done quickly as the quantity of solid nitrogen in the bucket is reduced over time as it sublimes. The following procedure is used to rapidly form the solid nitrogen:

i. Pump down chamber to pressure below 0.1 Pa
ii. Pump in liquid nitrogen to pre-cool bucket
iii. Turn on cryocooler
iv. Set the PI controller's setpoint to 70 K
v. Pump slowly on the liquid nitrogen in the bucket to quickly evaporate it and ensure the bucket is empty
vi. Once the cryocooler is maintaining a temperature of 70 K, re-fill the bucket with liquid nitrogen
vii. Set the PI controller's setpoint to 60 K
viii. Start pumping on the bucket to form solid phase
ix. When the bucket temperature reaches 60 K, control the pumping rate so that the temperature is maintained and perform experimentation

If the coldhead was at a warmer temperature than the bucket, heat would flow from the coldhead to the bucket. By running the cryocooler, the coldhead would be colder than the bucket, and it would the cooling process. Turning the cryocooler on and controlling the bucket base stops this from interfering with the results of the experimentation.

3.3 Pulse Experiment Descriptions

3.3.1 Transient Heating and Recovery Time

The power and recovery time experiments investigate how the solid nitrogen responds to transient heating of the resistor and allow the resistor to recover to the original operational temperature. The resistor used to simulate the normal state of a superconductor is subjected to multiple transient heating pulses, and the temperatures across it are measured using the probe shown in Figure 2.19. Varying the transient heating power and the duration of the pulses provides temperature variation data that will aid in thermal battery design for an SFCL. Performing these tests multiple times using solid nitrogen which has been solidified at different cooling rates should demonstrate how the cooling rate affects the quality of the thermal contact between the solid nitrogen and resistor.

A summary of the experimentation using different powers and durations tested for slow and quickly formed solid nitrogen are tabulated below. The number of sequential experiments performed for quickly formed solid nitrogen was much less than that of slowly formed solid nitrogen because the thermal contact deteriorated rapidly in the former case.

Several single pulse experiments were performed without solid nitrogen present. In this case the resistor and thermometers were cooled only by radiation between them and the bucket. The purpose of performing these experiments was to investigate the response when thermal contact is completely destroyed.

The pulse durations are not the typical duration a SFCL would incur. They have been selected purely for the purpose of evaluating the thermal battery. An SFCL would typically experience a much short pulse of greater magnitude.

Table 5 Heating and Recovery Experiments

SN_2 Formation Rate	Power (W_{RMS})	Pulse Duration (s)
Slow	1.9	1
		5
	8.4	0.25
		1
		5
	17	0.25
		1
		5
	30	0.25
		1
Fast	1.9	1
	8.4	1
Vacuum	1.9	5
	17	0.25

3.3.2 Dry-out

As there has not been much experimentation published regarding dry-out, data needs to be acquired so that predictions of the influence of multiple heating pulses on the thermal contact between the solid nitrogen and superconductor can be made. The purpose of performing these experiments is to observe the affect of the cooling rate during solidification of nitrogen on the occurrence of dry-out.

The thermal battery is subjected to multiple transient heating pulses. Pulses only occur once the battery has recovered to its original temperature. Recovery time and temperature variation are monitored to determine the extent of dry-out. Table 6 shows what dry-out experiments were performed. It gives the formation rate, power of each pulse, duration of each pulse and number of pulses which occurs.

Table 6 Dry-out Experiments

SN_2 Formation Rate	Power (W_{RMS})	Duration (s)	Pulses
Slow	1.9	1	11
	17	1	13
	30	1	7
		5	7
Fast	1.9	1	4

4 Results and Discussion

Having carried out the transient heat and 'dry-out' experiments, which were outlined in sections 3.3.1 and 3.3.2, the results are presented in this chapter with a discussion following each group of experiments.

4.1 Transient Heating and Recovery Time

4.1.1 Slowly Formed SN_2

The solid nitrogen used for the experiments in this section was slowly formed by cooling at a rate of -0.1 K/min between 66 K and 60 K.

Figure 4.1 shows the controlled cooling for slow cooled SN_2. The SN_2 is first cooled to, and idled at 66 K for 15 minutes then cooled to 60 K at a rate of -0.1 K/min.

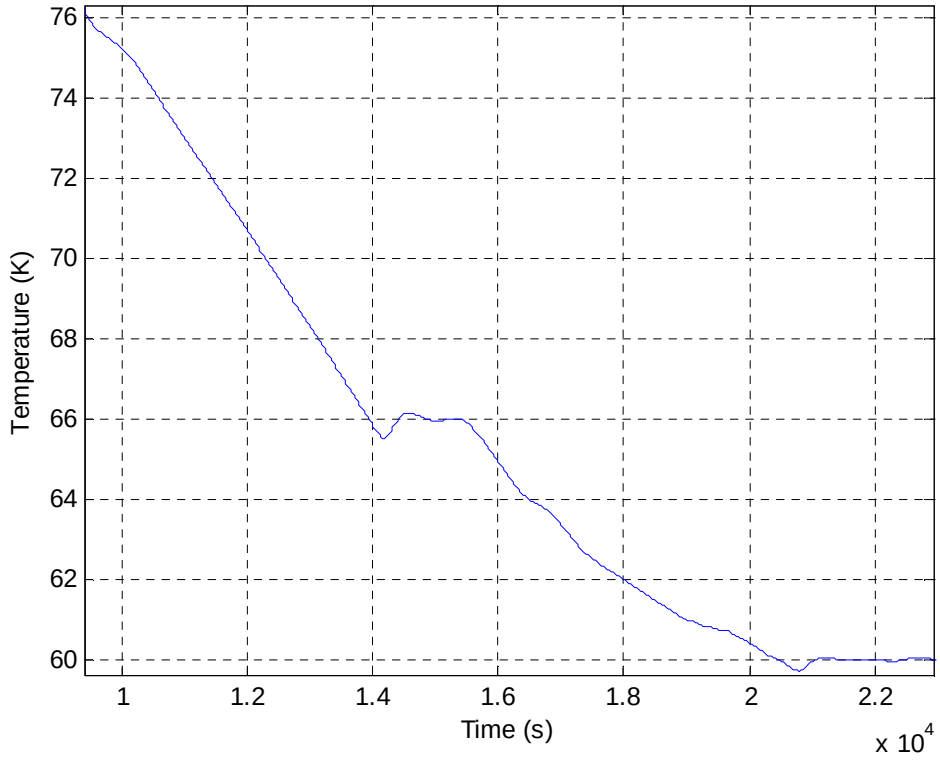

Figure 4.1 Time vs. Temperature of experimental stage showing cooling rate for slow cooled SN_2

Figure 4.2 shows the temperature response of the resistor to 1 s sequential pulses, varying the power of the pulse. The thermal stability which the solid nitrogen is providing can be seen in the first few seconds after the pulse with the rapid drop in temperature. Figure 4.3 shows that the maximum (peak) change in temperature as a function of power. Measured recovery times to 60.15 K are shown in Figure 4.4.

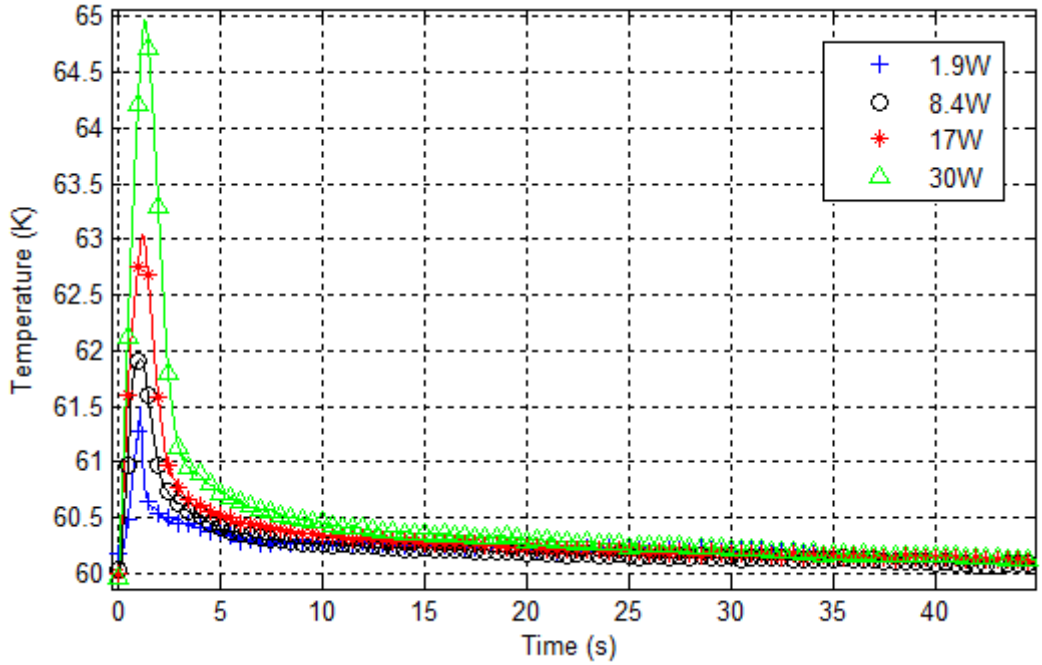

Figure 4.2 Time vs. Resistor Temperature, varying the power for 1s pulse, slowly formed SN_2

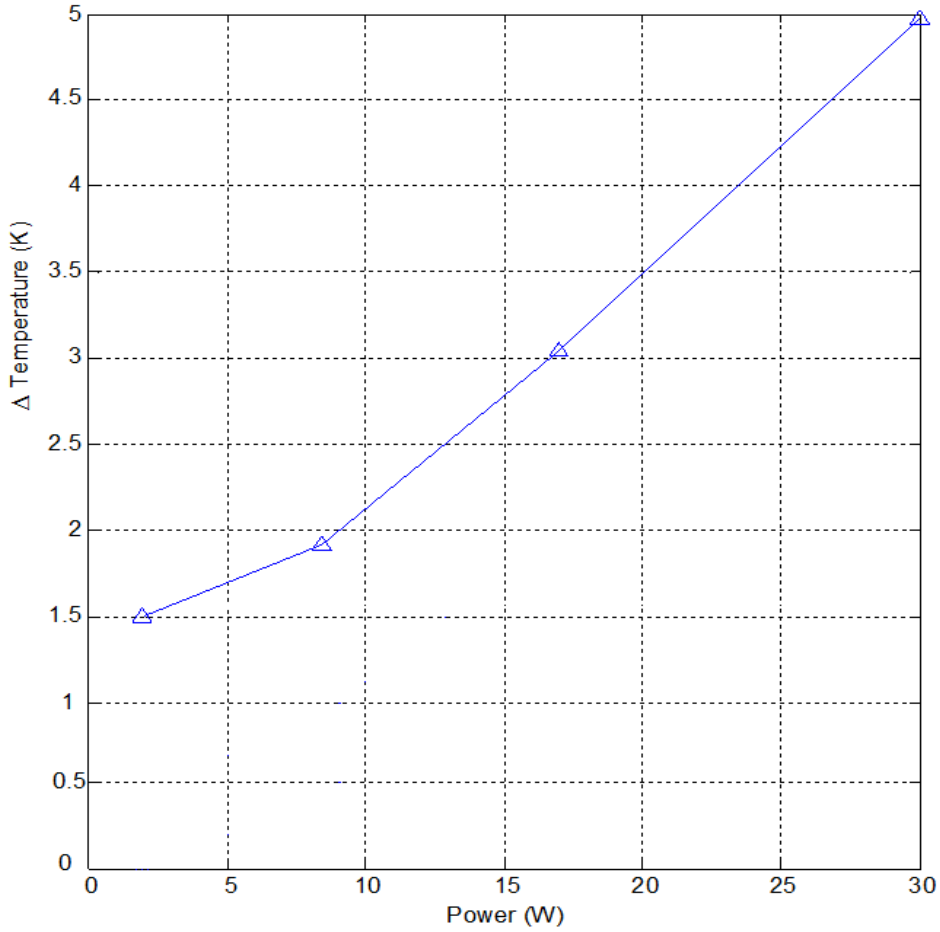

Figure 4.3 Power vs. Change in temperature comparison for slowly formed SN_2

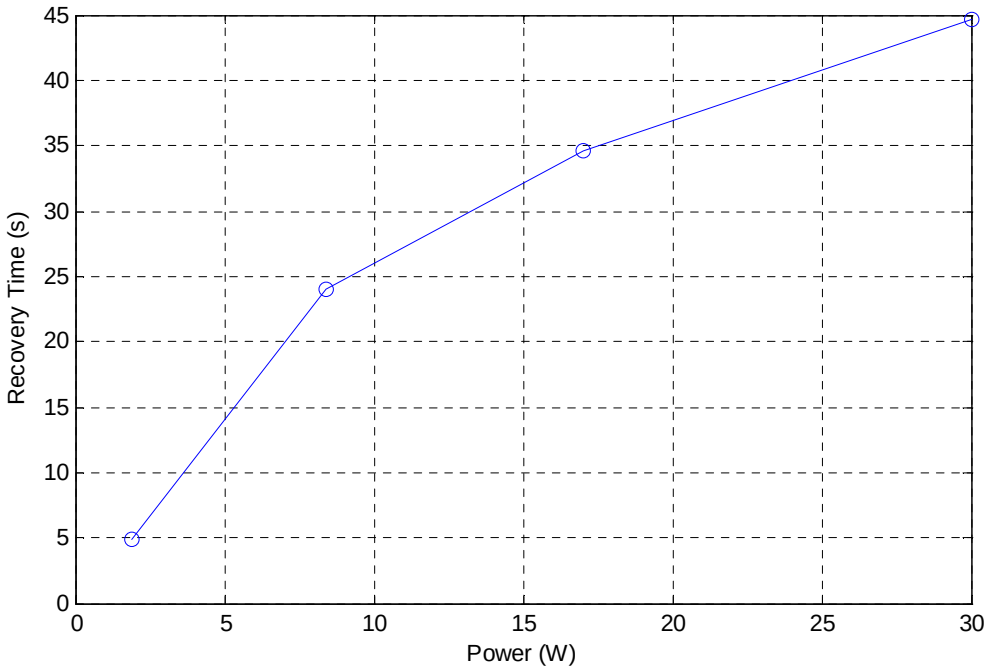

Figure 4.4 Power vs. Recovery Time to 60.15 K for slowly formed SN_2

Figure 4.5 shows temperature variation due to transient heating as it affected the whole thermal battery after it was subjected to a 30 W pulse of 1 s duration. The plot gives the temperature of several locations on the probe. For visualization purposes a sketch of the probe is provided on the plot. The temperature of the resistor (Thermometer 1) stabilizes[10] in 2 s, after which the temperatures across the thermal battery are equal. Once the temperatures are equal the time it takes to recover to 60 K is dependent on the cryocooler and available cooling power at this temperature. It can be seen that the temperature of the resistor exceeds the melting point of solid nitrogen (T_m = 63.15 K) and it is likely that repetitive pulses of this power and/or duration would probably lead to 'dry-out'.

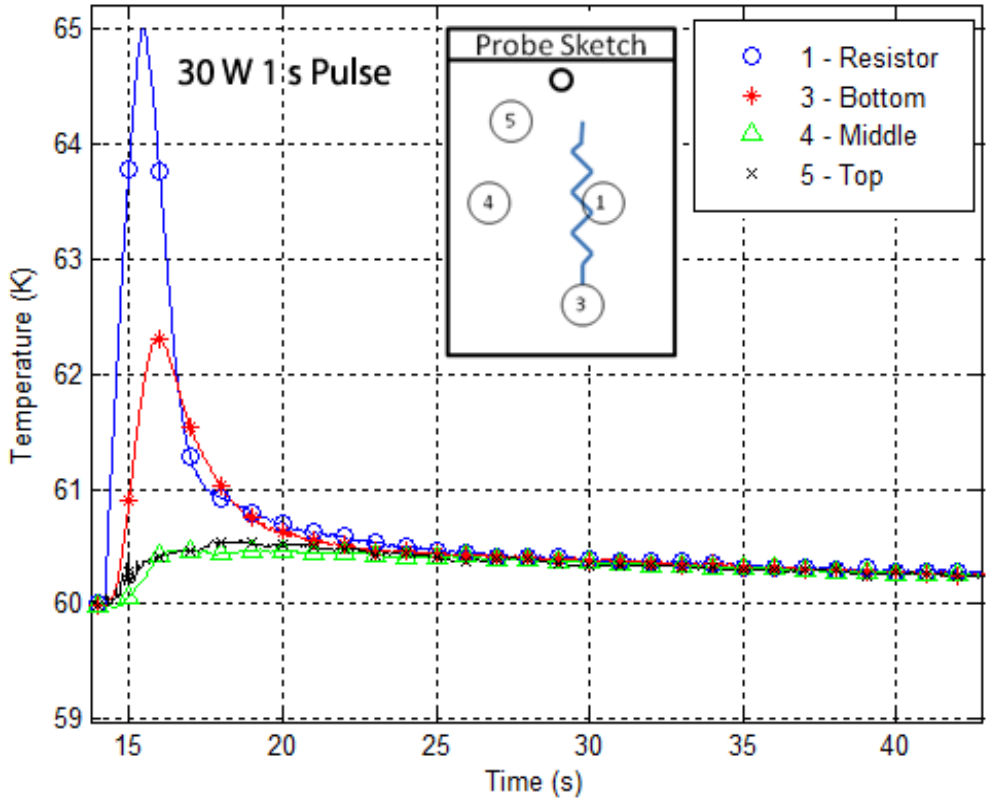

Figure 4.5 Time vs. Temperature response of resistor for 30 W Pulse of 1s duration for Slowly Formed SN_2

4.1.2 Rapidly Formed SN_2

The rapidly formed solid nitrogen was cooled at a rate of -1.99 K/min between 64 K and 62 K by pumping on the liquid until it solidifies and reaches the desired temperature. To maintain the temperature and solid phase the rotary pump is left running. The cryocooler is

[10] Recovered by 80 % of the change in temperature

also still running throughout the experiment. Figure 4.6 shows the cooling process for rapidly formed SN_2.

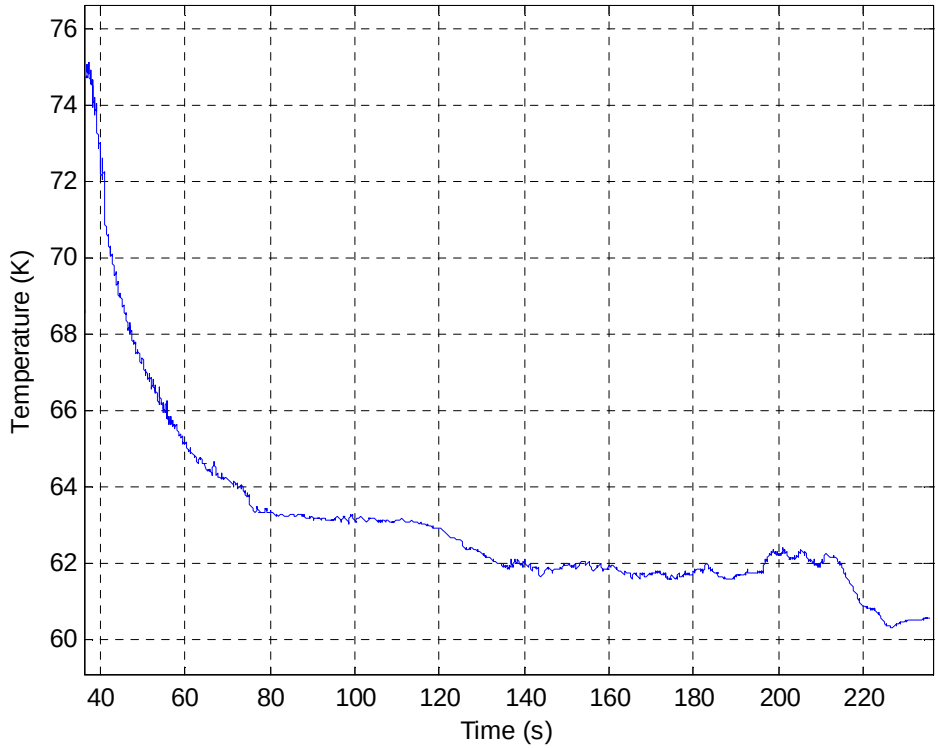

Figure 4.6 Time vs. Temperature of resistor showing formation of rapidly cooled SN_2

Figure 4.7 shows the resistor's temperature response to a 1.9 W pulse of 1 s duration. The 'pulse' plot indicates the period for which the pulse occurred, and the amplitude is not scaled to any particular value. The provision of additional cooling power through the sublimation process (solid to gas) is a possible reason for the peak temperature being lower than that of the slowly formed solid nitrogen. The time the thermal battery took to recover to 60.6 K was 33 s. This is much longer than some liquid nitrogen cooled SFCL's which are capable of recovering in 0.5 s to 5 s [16]. The thermal battery's response to the transient heating was gradual and it remained in the region of its peak temperature for 12 s.

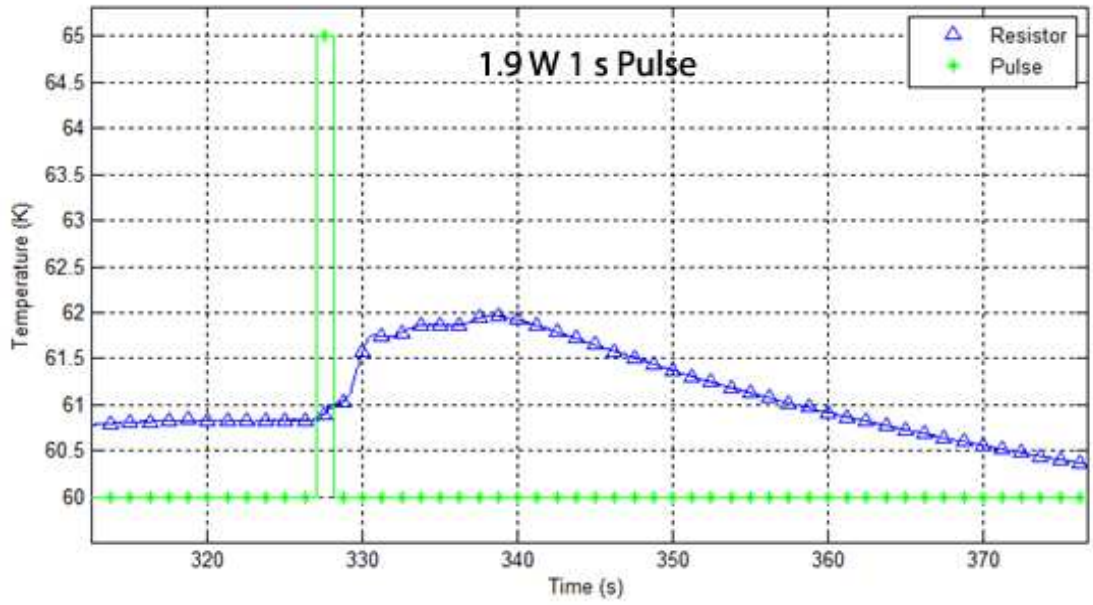

Figure 4.7 Time vs. Temperature of the resistor (Thermometer 1) for 1.9 W pulse of 1 s duration in rapidly formed SN_2

4.1.3 Absence of SN_2

Experimentation done in the absence of solid nitrogen provides an indication of the thermal response when there is no longer thermal contact between the solid nitrogen and resistor. A rotary pump is connected to the liquid nitrogen inlet pipe and the bucket is placed under vacuum. Figure 4.8 and Figure 4.9 show the response for thermal transients of different powers and durations. Clearly both figures are following a similar trend, with differences being that of scale as each is subjected to different average powers.

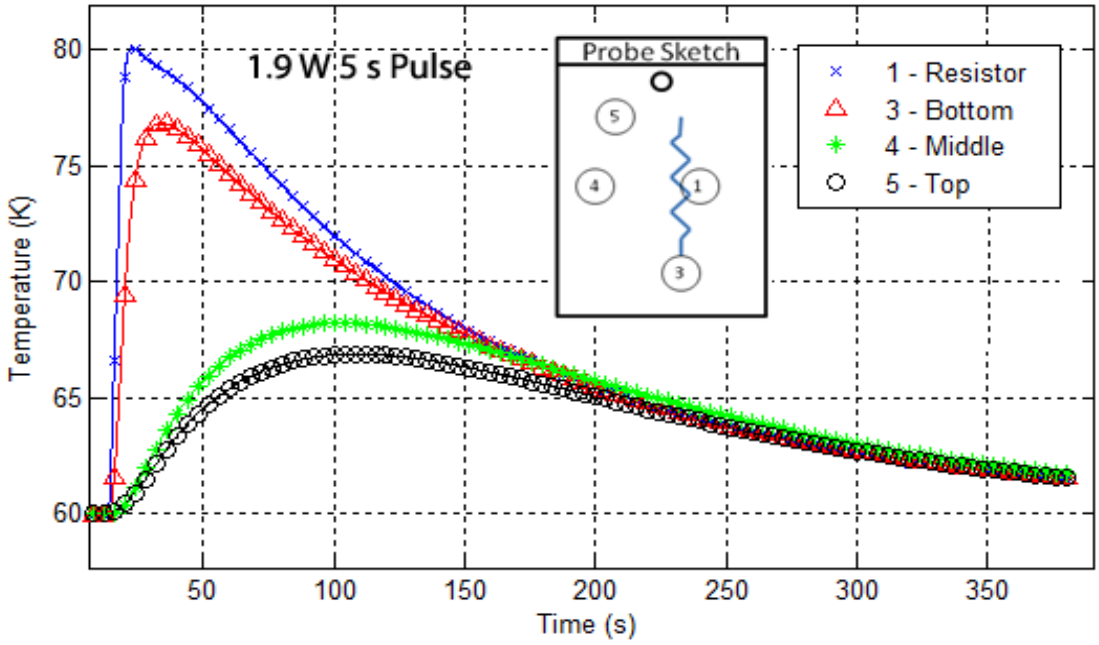

Figure 4.8 Time vs. Temperature for 1.9 W pulse of 5 s duration in vacuum

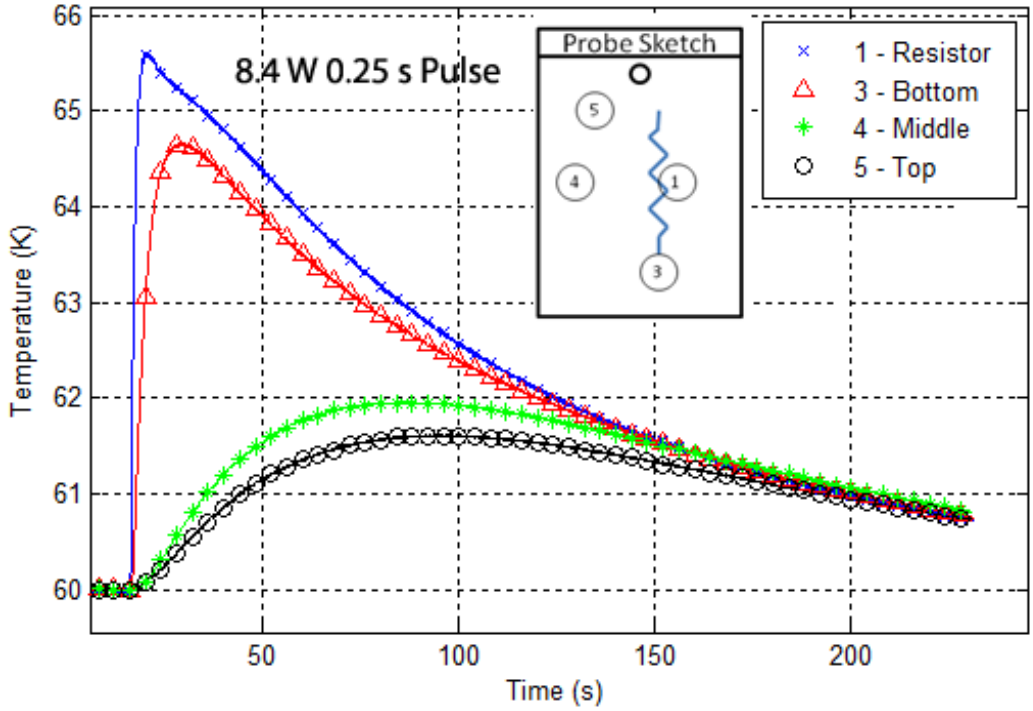

Figure 4.9 Time vs. Temperature for 8.4 W pulse of 0.25 s duration in vacuum

4.1.4 Discussion and Comparisons

Figure 4.10 below shows a comparison between the thermal responses of solid nitrogen at two different solid nitrogen formation rates when subjected to a 1.9 W pulse of 1 s duration.

There are several clear differences between the two sets of data. The slow cooled SN_2 temperature measurement seems to respond must sooner after the transient had occured and subsequently track it better, but peaks 0.2 K higher than fast cooled SN_2.

The fast cooled SN_2 doesn't follow this trend. As previously mentioned, one must continue pumping on the solid nitrogen to maintain a set temperature. The cooling provided from the phase change to gas seems to reduce the initial gradient of the response and is responsible for the constant cooling gradient seen between 12 s and 30 s. It is likely that the reason this phase change is more efficient than that of slowly formed solid nitrogen is because the rotary pump is still running and maintaining a low pressure environment which the quickly formed solid nitrogen is in. From a response time perspective the more gradual change during the first 4 s may seem advantageous, but the plateau-like region which lasts for 8 seconds that follow is not.

The slow cooled SN_2 stabilizes the temperature of the resistor much faster showing the improvement of thermal contact between it and the solid nitrogen.

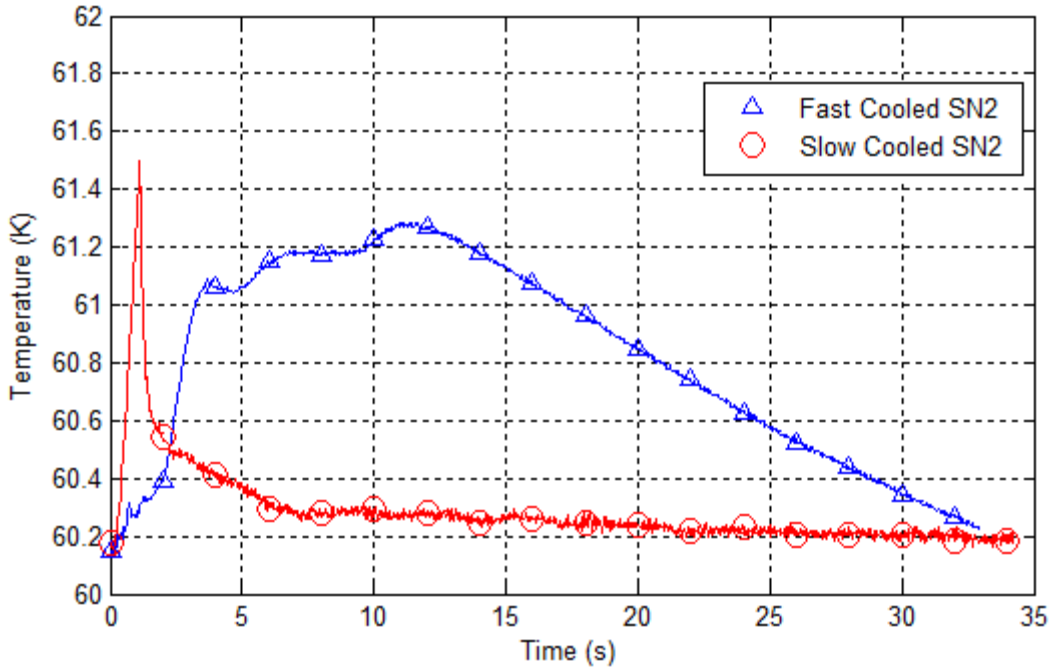

Figure 4.10 Time vs. Temperature of resistor comparing different cooling rates for 1.9 W pulse of 1 s duration

Figure 4.11 compares the thermal response between using solid nitrogen to provide cooling to a response when the thermal contact has deteriorated (vacuum). This highlights the importance of ensuring that a complete deterioration of thermal contact does not occur. In the situation when thermal contact has deteriorate, the temperature response of the resistor (or superconductor) would be 6.2 times larger. Recovery time can also be seen to have lengthened considerably.

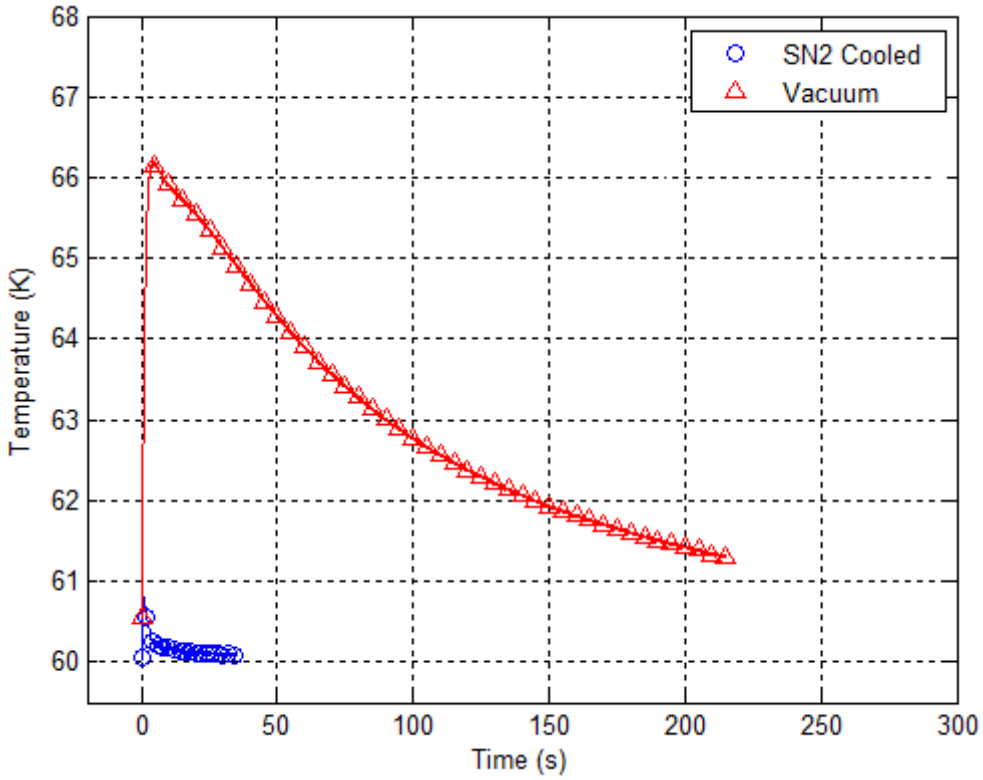

Figure 4.11 Graph of Time vs. Temperature comparing SN_2 cooling to vacuum

4.2 Dry-out

4.2.1 Slowly formed SN_2 at 60K

The slowly formed solid nitrogen used for the dry-out experimentation was cooled at an average rate of -0.026 K/min between 63.5 K and 60.3 K.

Figure 4.12 shows the resistors temperature response using slow formed SN_2 when subjected to multiple heating pulses at 1.9 W. The thermal battery performs consistently throughout.

Dry-out does not seem to be detectable after 11 pulses as the recovery time and change in temperature hasn't changed significantly.

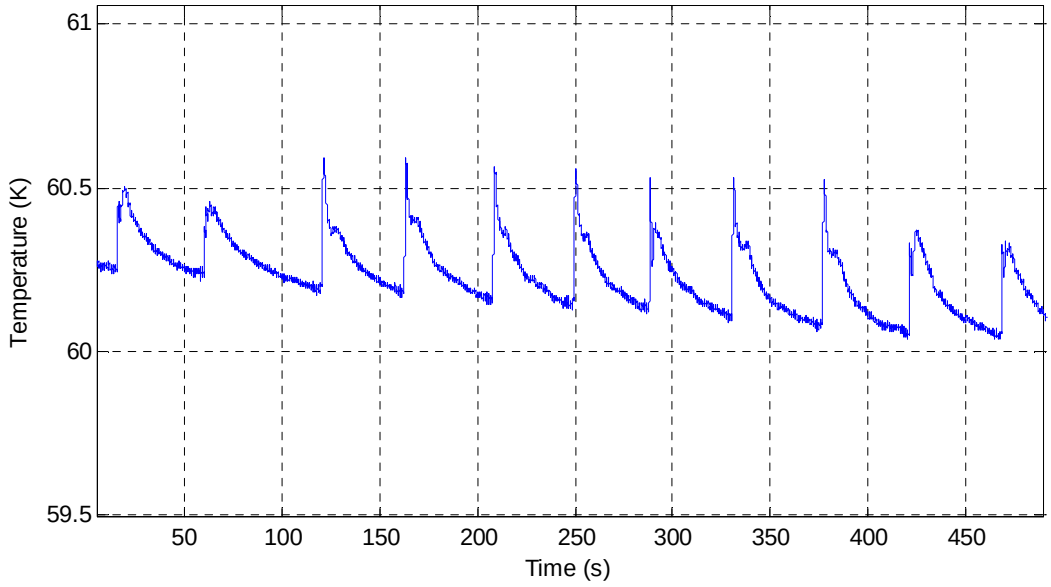

Figure 4.12 Time vs. Temperature of the resistor for 1.9 W pulses of 1 s duration, slowly formed SN_2

Figure 4.13 shows temperature response of the resistor using slow formed SN_2 after being subjected to 13 pulses of 17 W and 1 s duration. The change in temperature for each pulse seems to be fairly consistent, but the recovery time gradually increases after each successive pulse.

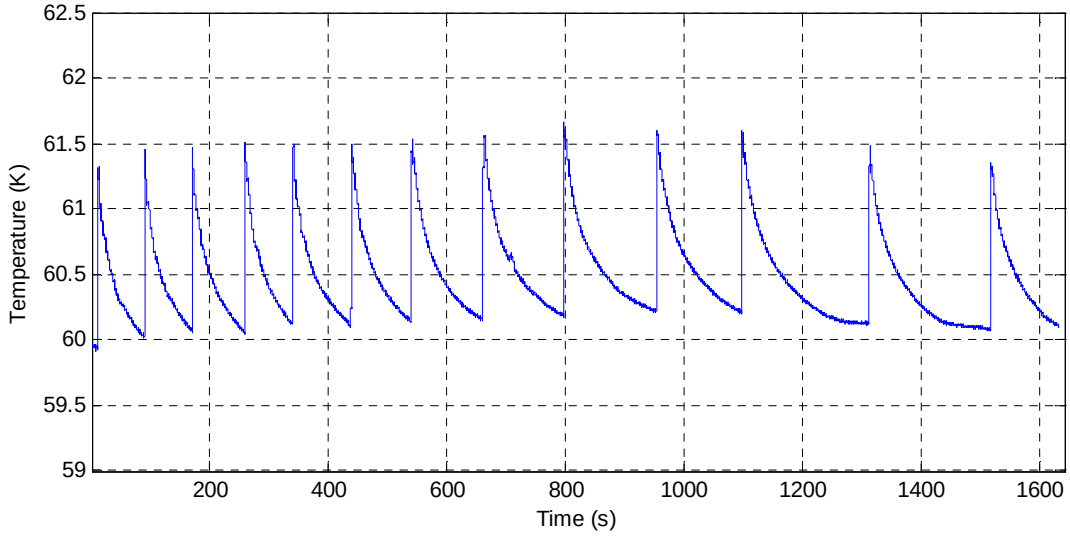

Figure 4.13 Graph of Time vs. Temperature of the resistor for 17 W pulses of 1s duration, slowly cooled SN2

4.2.2 Rapidly formed SN_2 at 60K

The solid nitrogen was rapidly formed at a rate of -1.99 K/min. Figure 4.14 shows the temperature response of the resistor when subjected to 1.9 W pulses of 1 s duration. The response worsens after each pulse, with the change in temperature (ΔT) and response time increasing. The initial pulse has the lowest ΔT and recovery time. The reduction in performance for the 2nd pulse is significant. After the 3rd pulse there is a small plateau around 63 K, which could indicate the some of the solid nitrogen has melted and is refreezing, this would be due to the 'pooling' of liquid nitrogen around the resistor and freezing. The 4th pulse's recovery starts to mimic the response for pulses done in the absence of SN_2 (Section 4.1.3).

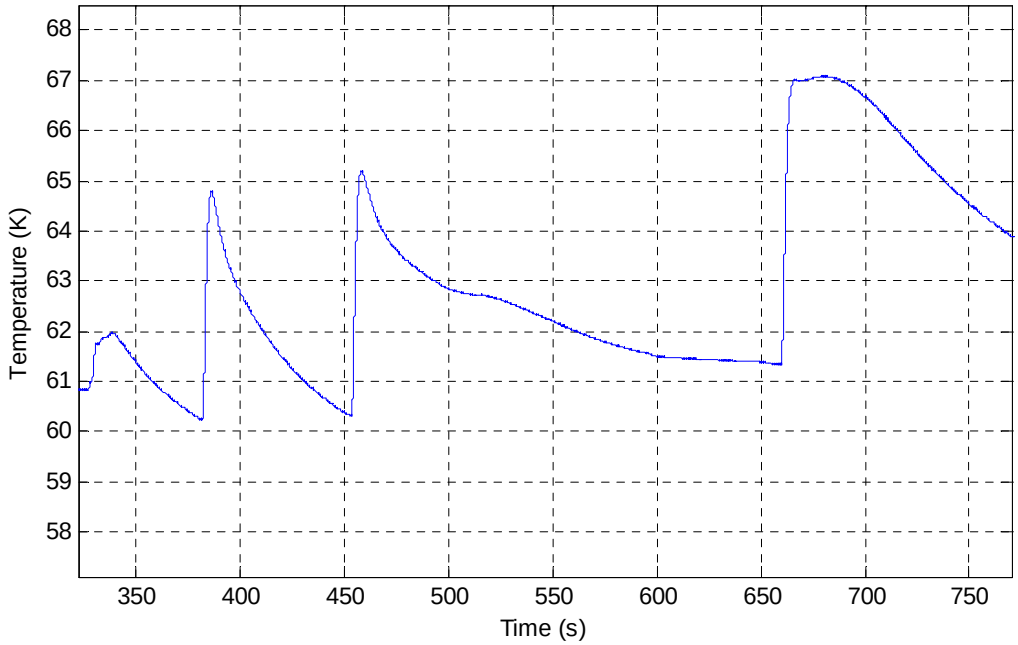

Figure 4.14 Graph of Time vs. Temperature for 1.9 W pulses of 1 s duration, fast cooled SN_2

4.2.3 Discussion

Comparisons of the change in temperature and recovery time after each successive 1 s pulse at 1.9 W for slow and fast cooled SN_2 are shown in Figure 4.15 and Figure 4.16. Dry-out seems to begin after the first pulse for fast cooled SN_2. Changes in both temperature and recovery time increase significantly for the fast cooled SN_2. This response is not seen for the slow cooled SN_2. When subjected to identical pulses in power and duration it performs consistently with minimal variation in both temperature change and recovery time.

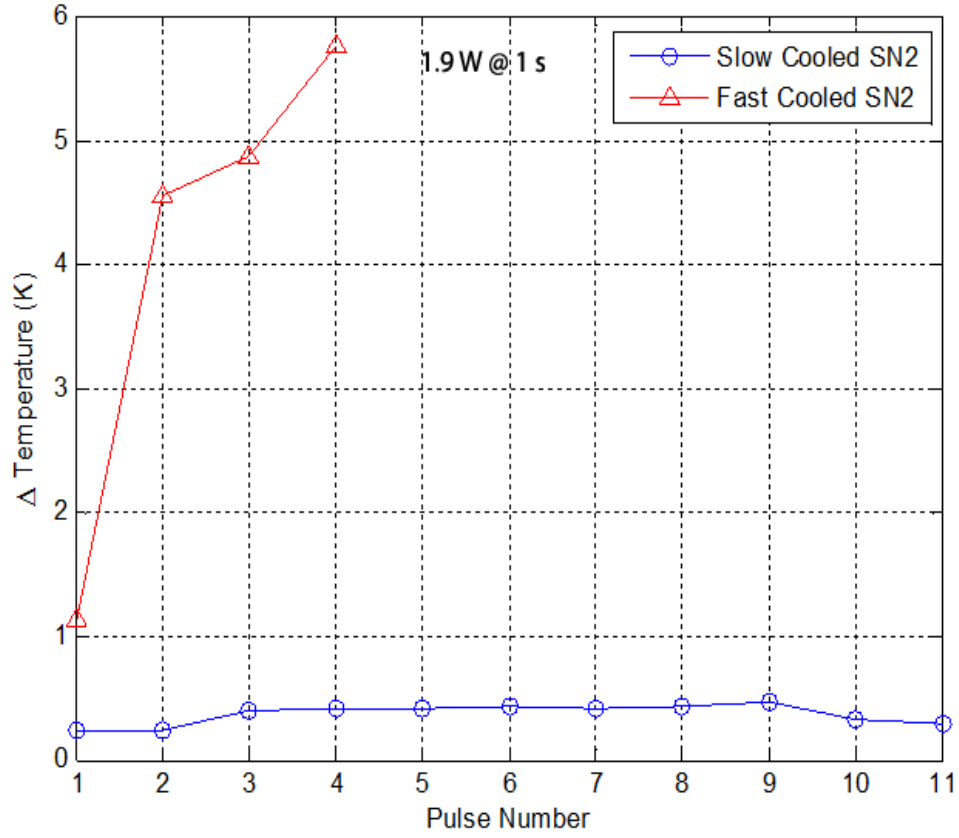

Figure 4.15 Pulse Number vs. Δ Temperature comparing Fast and Slow Cooled SN_2, investigating dry-out

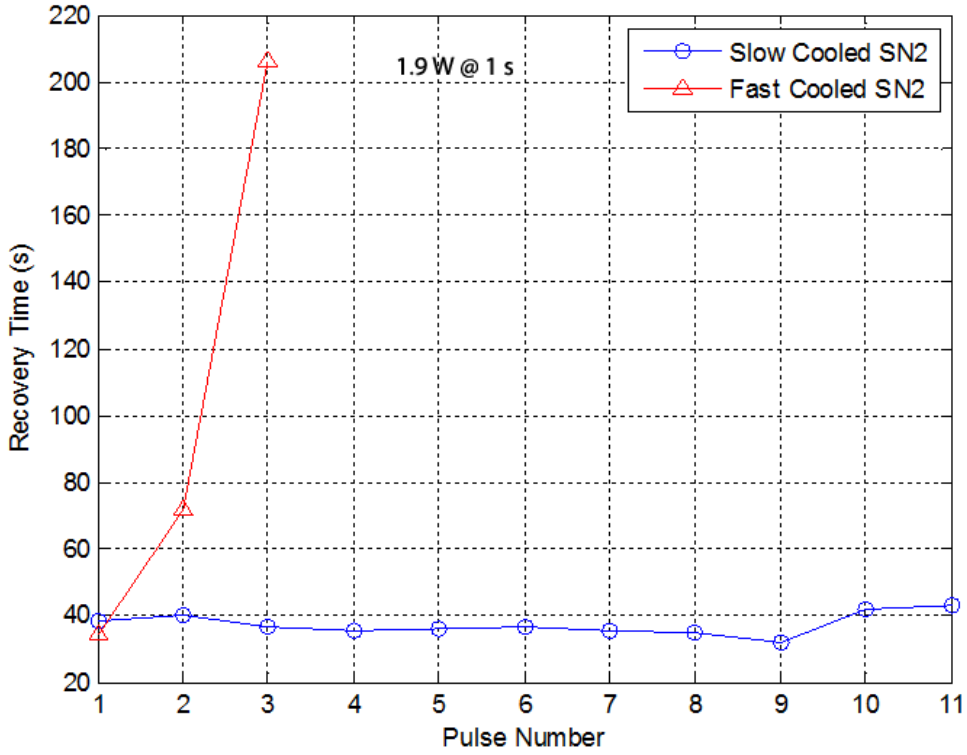

Figure 4.16 Pulse Number vs. Recovery Time comparing Fast and Slow cooled SN_2, investigating dry-out

Figure 4.17 and Figure 4.18 compare the change in temperature and recovery time for slow cooled SN_2 with different pulse powers. The trends on Figure 4.17 are fairly consistent with one another.

It is interesting to note the dip in both recovery time and change in temperature towards the end of the set of pulses on both figures. The reason for this is not clear from the data obtained and additional experiments are required to clarify the cause. The initial temperature for the end pulses was slightly lower than for previous pulses which is possibly the reason for this change. Another possibility is that the heating of the resistor is not distributed uniformly across it and regions are reaching temperatures at which the solid nitrogen is melting, and subsequently refreezing. This melting and refreezing process may be causing the liquid nitrogen to pool in certain regions and refreeze with better thermal contact than it had previously.

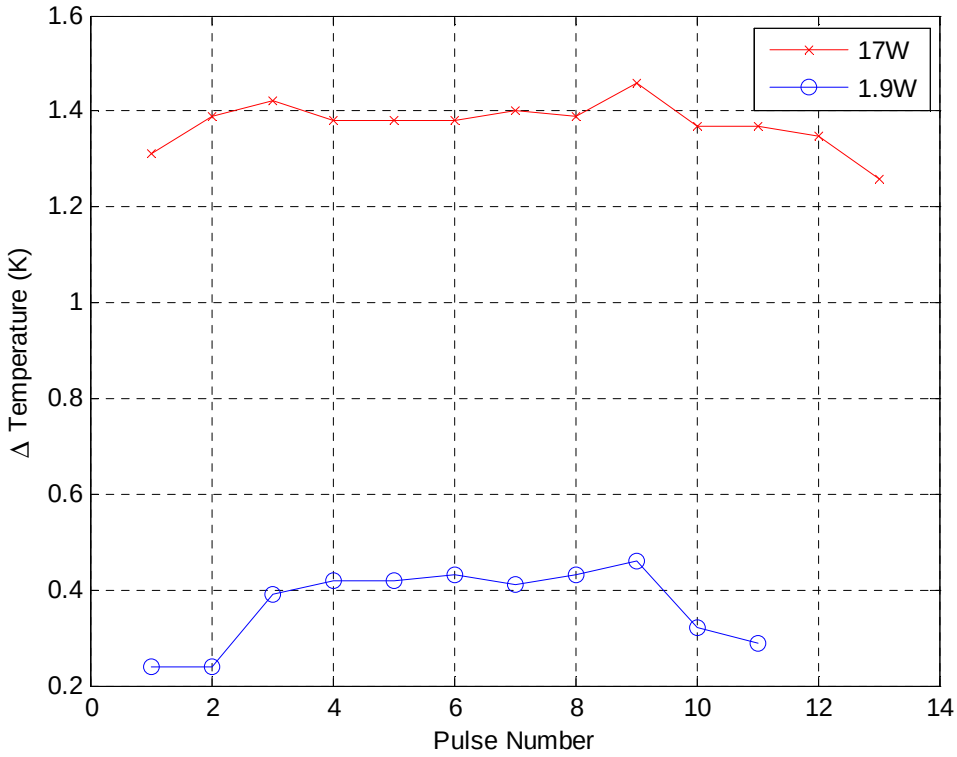

Figure 4.17 Graph of Pulse Number vs. Δ Temperature for different powers of slow cooled SN_2

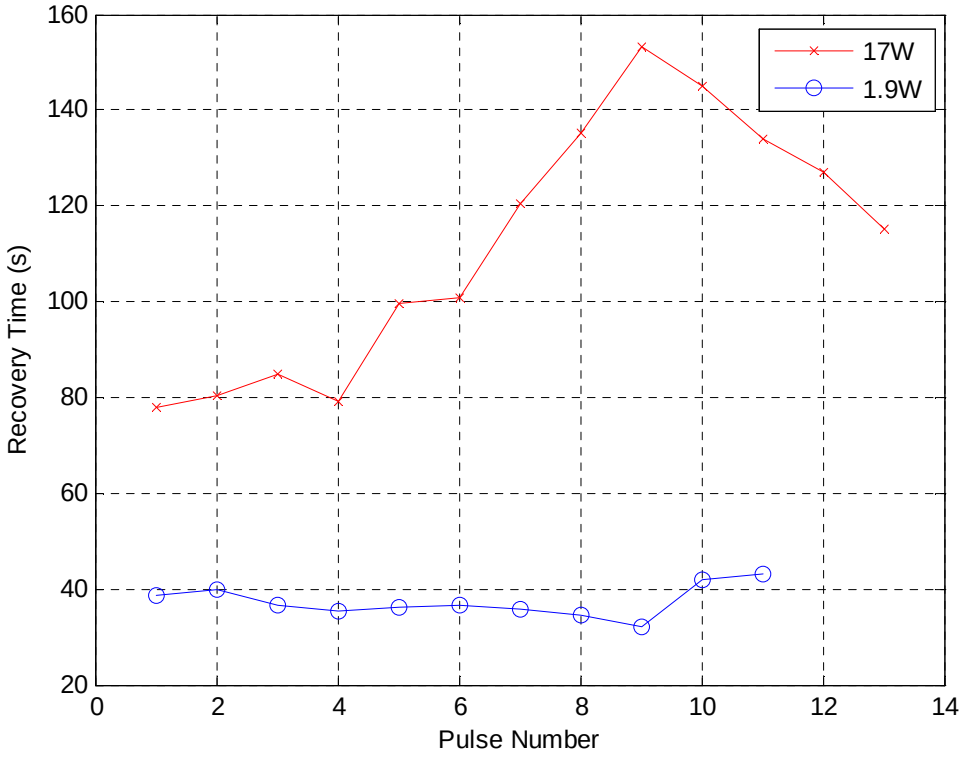

Figure 4.18 Graph of Pulse Number vs. Recovery Time for different powers of slow cooled SN_2

4.3 Chapter Conclusions

Comparison graphs of the thermal response and dry-out testing both show the improvement of using solid nitrogen formed at a slow rate.

The thermal response of slowly formed solid nitrogen during transient heating pulses stabilises the resistor temperature much quicker than using solid nitrogen formed at a faster rate. There does appear to be some benefit of pumping on the solid nitrogen, where pockets of solid nitrogen liquefy and evaporate providing additional cooling power.

Dry-out was an issue when the solid nitrogen was formed quickly with both the change in temperature and recovery time rising rapidly after each successive pulse. It did not seem to be present when formed slowly even though it was subjected to a series of pulses between 1.9 W and 17 W.

There are several experiments noted in this chapter which can be performed to clarify some of the results and to carry this research further, providing a better understanding of the dependence of thermal contact resistance on formation rate for solid nitrogen.

5 Future Work

5.1 Thermal Battery Improvements

Controlling the cooling rate when forming solid nitrogen was found to improve the thermal contact resistance and allow the thermal battery to perform better. There are several methods which are likely to further improve its performance.

5.1.1 Pressurised Thermal Battery

Researchers have already shown that pressurising the thermal battery with neon gas improves its performance [41]. This was found in the process of forming a hybrid refrigerant (a mixture of solid nitrogen and liquid neon).

It is believe that if the thermal battery was pressurised with a more thermally conductive gas such as helium, the improvement to performance would be greater. Using a combination of helium and neon gas would allow for a hybrid refrigerant to be formed as well.

5.2 Scaling up for High Current Tests

The design of the cryostat and thermal battery needs to be scaled up for higher current testing. Using a cryocooler with greater cooling power to form a larger thermal battery is paramount if the battery is to be used practically in-conjunction with a superconducting FCL.

5.2.1 2G HTS Current Leads

Higher current pulses would require thicker copper current leads to minimise joule heating, yet doing so increases the heat flow into the experimental stage of the cryostat significantly Alternatively, Second generation High Temperature Superconducting (2G HTS) wire should be used for current leads between the first and second stage (experimental stage) of a cryocooler's coldhead. The superconductor's properties of zero resistance in the superconducting state and low thermal conductivity make it an ideal choice to minimize heat flow into the experimental stage [42]. 2G HTS wire was found to be up to 3 times less thermally conductive than 1G wire and at least 10 times less than copper.

5.2.2 Modelling of Thermal Battery

The quantity and cooling rate of the thermal battery refrigerant needs to be determined, ensuring that the thermal transient is adequately suppressed, and dry-out does not occur. It would be beneficial to predict the thermal contact resistance based on transient heating data.

Using the thermal contact resistance prediction, the thermal battery can be modelled and its response during quench predicted.

6 Conclusions

The Superconducting Fault Current Limiter is a novel solution to the problem of limiting fault currents. As the cost of High Temperature Superconductors, e.g. Magnesium Diboride and cryocoolers falls, the SFCL becomes more attractive. The likelihood of it being commercialised and utilised should increase as it is refined through research [22, 24, 34].

The focus of this dissertation has been on the design of a cryostat for the study of thermal battery. The cryostat was successfully designed and built. When unloaded by an experimental stage, the 2nd stage of the cold finger was capable of temperatures below 20 K. The experimental stage was only able to reach 82 K when connected without a thermal radiation shield. Following the implementation of the superinsulated radiation shield, the experimental stage was capable of reaching 40 K. This was adequate to solidify nitrogen and test its use as a thermal battery.

The thermal battery was tested by pulsing a resistor with surge currents to generate transient heating events. This simulated the transition of a superconductor to its normal state, when a fault occurs. The thermal response to the heating events of the resistor and surrounding solid nitrogen were measured for different formation rates of the solid nitrogen. It was shown that slowly cooling solid nitrogen during solidification improved the performance of the thermal battery. This improvement is credited to an improvement of thermal contact between the solid nitrogen and the surfaces it's in contact with.

The phenomenon of "dry-out" was also investigated. It was immediately noticeable when testing rapidly formed solid nitrogen with consecutive low power (1.9 W) pulses of 1s duration. Testing slow formed solid nitrogen did not produce any 'dry-out' behaviour. Even at higher powers (17 W) dry-out was not detected for slowly cooled solid nitrogen.

The solid nitrogen thermal battery experiments show it to be a promising method of absorbing the heat generated when a superconductor quenches. As improvements are made to the thermal contact resistance between the solid nitrogen and contact surfaces, the performance of the battery will improve, reducing the change in temperature and recovery times.

The prototype cryostat is now ready for testing with BSSCO wire/tape using the solid nitrogen thermal battery. To test MgB_2 wire/tape, a higher powered cryocooler would need to be used.

References

[1] H Isogami, B Haid, and Y Iwasa, "Thermal behavior of a solid nitrogen impregnated high-temperature superconducting pancake test coil under transient heating," *IEEE Trans. Appl. Supercond.*, vol. 11, no. 1, pp. 1852-1855, 2001.

[2] B Haid, H Lee, Y Iwasa, and et. al., "A "permanent" high-temperature superconducting magnet operated in thermal communication with a mass of solid nitrogen," *Cryogenics*, vol. 42, pp. 229-244, 2002.

[3] J G Hartnett, P Y Bourgeois, J D Anstie, and M E Tobar, "High-Q frequency-temperature compensated solid-nitrogen-cooled resonator-oscillators: first results," *Electronics Letters*, vol. 40, no. 1, pp. 41-42, 2004.

[4] P Hales, H Jones, S Milward, and S Harrison, "Investigation into the use of solid nitrogen to create a "Thermal Battery" for cooling a portable high-temperature superconducting magnet," *Cryogenics*, vol. 45, no. 2, pp. 109-115, 2005.

[5] A Sugawara, H Isogami, B Haid, and Y Iwasa, "Benificial effect of solid nitrogen on a BSCCO-2223/Ag composite tape subjected to local heating," *Physica C*, vol. 372, pp. 1443-1446, 2002.

[6] T Nakamura, I Muta, K Okude, and et. al., "Solidifcation of Nitrogen Refrigerant and its effect on thermal stabilty of HTSC tape," *Physica C*, vol. 372, pp. 1434-1437, 2002.

[7] T Manabe, T Nakamura, and Y Yamada, "Heat transfer characteristics of HTS tape impregnated with solid nitrogen-solid neon hybrid refrigerant," *Physica C*, vol. 468, pp. 2156-2160, 2008.

[8] T Nakamura et al., "Improvement of dissipative property in HTS coil impregnated with solid nitrogen," *Physica C*, vol. 386, pp. 415-418, 2003.

[9] T Nakamura, K Higashikawa, I Muta, and et. al., "Performance of conduction-cooled HTS tape with the aid of solid nitrogen-liquid neon mixture," *Physica C*, vol. 412, pp. 1221-1224, 2004.

[10] J B Williamson, J Pullen, T R Hunt, and D Leonard, "The Shape of Solid Surfaces," *Surface*

Mechanics, American Society of Mechanical Engineers, pp. 24-35, 1969.

[11] M Bahrami, J R Culham, M M Yovanovich, and G E Schneider, "Thermal contact resistance of nonconforming rough surfaces, part 1: contact mechanics model," *Journal of Thermophysics and Heat Transfer*, vol. 18, no. 2, pp. 209--217, 2004.

[12] Jack W. Ekin, *Experimental Techniques for Low-Temperatuer Measurements*.: Oxford University Press, 2007.

[13] L J Salerno and P Kittle, "Thermal Contact Conductance," *NASA Technical Memorandum*, no. 110429, February 1997.

[14] L J Salerno, P Kittle, and A L Spivak, "Thermal conductance of metallic contacts augmented with Indium foil or Apiezon N grease at liquid Helium temperatures," *Cryogenics*, vol. 34, no. 8, pp. 649-654, 1994.

[15] M Bahrami, J R Culham, M M Yovanovich, and G E Schneider, "Thermal contact resistance of nonconforming rough surfaces, part 2: Thermal model," *Journal of Thermophysics and Heat Transfer*, vol. 18, no. 2, pp. 218--227, 2004.

[16] A L Jarvis, "Superconductivity ENEL4SC - Lecture Notes,".

[17] T V Ramakrishnan and C N Rao, *Superconductivity Today - An Elementary Introduction*. New Delhi: Wiley Eastern Limited, 1992.

[18] (2011, Jan) AccessScience from McGrawHill. [Online]. http://www.accessscience.com/loadBinary.aspx?filename=YB001430FG0010.gif

[19] Andrei Mourachkine, *Room-Temperature Superconductivity*.: Cambridge International Science Publishing, 2004.

[20] M. Brown, R. Balakrishnan L.G. Hewitson, *Practical Power System Protection*.: Elsevier, 2005.

[21] S S Kalsi and A Malozemoff, "HTS Fault Current Limiter Concept," *Power Engineering Society General Meeting, 2004. IEEE*, pp. 1426--1430, 2004.

[22] S Eckroad, "Survey of Fault Current Limiter (FCL) Technologies," EPRI, California, 2008.

[23] ABB. (2010, Dec) ABB Is-Limiter - Fault Current Limitation. [Online]. http://www.abb.co.za/product/db0003db004279/c125739900636470c125698c00553a43.aspx

[24] N K Fall and B Marchionini, "Fault Current Limiter – R&D Status and Testing," in *Power Systems Conference and Exposition, 2009. PSCE'09. IEEE/PES*, 2009, pp. 1-4.

[25] A Neumann, "Application of Fault Current Limiters," *Department of Business Enterprise and Regulatory Reform*, 2007.

[26] L Ye, L Lin, and K Huengst, "Application studies of superconducting fault current limiters in electric power systems," *IEEE Transactions on Applied Superconductivity*, vol. 12, pp. 900-903, 2002.

[27] M Chen et al., "6.4 MVA resitive fault current limiter based on Bi-2212 superconductor," *Physica C*, vol. 372, pp. 1657-1663, 2002.

[28] T Yazawa et al., "Short circuit experiment on an FCL coil wound with YBCO tape with a high-resistance stabilizing layer," *Journal of Physics: Conference Series*, vol. 97, pp. 1 - 5, 2008.

[29] J Nagamatsu, N Nakagawa, T Muranaka, Y Zenitani, and J Akimitsu, "Superconductivity at 39 K in magnesium diboride," *Nature*, vol. 410, pp. 63-64, 2001.

[30] S R Das, "The Sensible Superconductor," *IEEE Spectrum*, vol. 39, no. 7, pp. 34-37, July 2002.

[31] Xiao Ji Dua, Qing Bao, Ling Qi Kong, Li Yang Ye, Li Ye Xiao Xiao Hang Li, "Design, development and experiment of a 1.5 T MgB2 superconducting test magnet," *Cryogenics*, vol. 49, pp. 286--290, 2009.

[32] L Ye, M Majoros, T Coombs, and et. al., "Experimental studies of the quench behaviour of MgB2 superconducting wires for fault current limiter applications," *Superconductor Science and Technology*, vol. 20, pp. 621-628, 2007.

[33] G Giunchi, G Ripamonti, T Cavallin, and E Bassani, "The reactive liquid Mg infiltration process to produce large superconducting bulk MgB2 Manufacts," *Cryogenics*, vol. 46, pp. 237-242, 2006.

[34] Y Cointe, P Tixador, and C Villard, "FCL: A solution to fault current problems in DC networks," *IOP - Journal of Physics: Conference Series 97*, 2008.

[35] (2010, February) Lake Shore Cryotronics. [Online]. http://www.lakeshore.com/pdf_files/Appendices/LSTC_appendixE_l.pdf

[36] Inc Cryomech, GB15 Cryo-refrigerator Capacity Curve, 09 May 2007.

[37] Wikipedia. [Online]. http://en.wikipedia.org/wiki/File:Conflat_Flange.jpg

[38] J C Archer, Designed and Built Desktop Tester Pulse Equipment - Superconductor Critical Current Testing.

[39] "Basics of Linear Fixed Resistors," Vishay Beyschlag, Application Note 2008.

[40] Lakeshore. (2010, October) Platinum RTDs. [Online]. http://www.lakeshore.com/pdf_files/sensors/LSTC_Platinum_l.pdf

[41] K Higashikawa and T Nakamura, "Cooling performance of hybrid refrigerant of solid nitrogen and small amount of neon for the purpose of HTS power applications," *Physica C*, vol. 429, pp. 1910 - 1914, 2009.

[42] C Hoffmann et al., "Thermal conductivity of 2G HTS wires for current lead applications," in *EUCAS*, 2010.

[43] J B Song, K L Kim, K J Kim, and J H Lee, "The design, fabrication and testing of a cooling system using solid nitrogen for a resistive high-Tc superconducting fault current limiter," vol. 21, pp. 1-8, 2008.

Appendix A - Volumetric Heat Capacity Calculations

A.1 Nitrogen

Figure A. 1 shows the volumetric heat capacity curve for nitrogen including the liquid-solid phase change at 63K and the alpha-beta solid phase change at 35.6 K [43]. Table A. 1 shows the values of the latent heats for nitrogen [12]. It is important to consider the volumetric heat capacity rather than the specific heat capacity so that one looks to maximise the heat capacity per unit area.

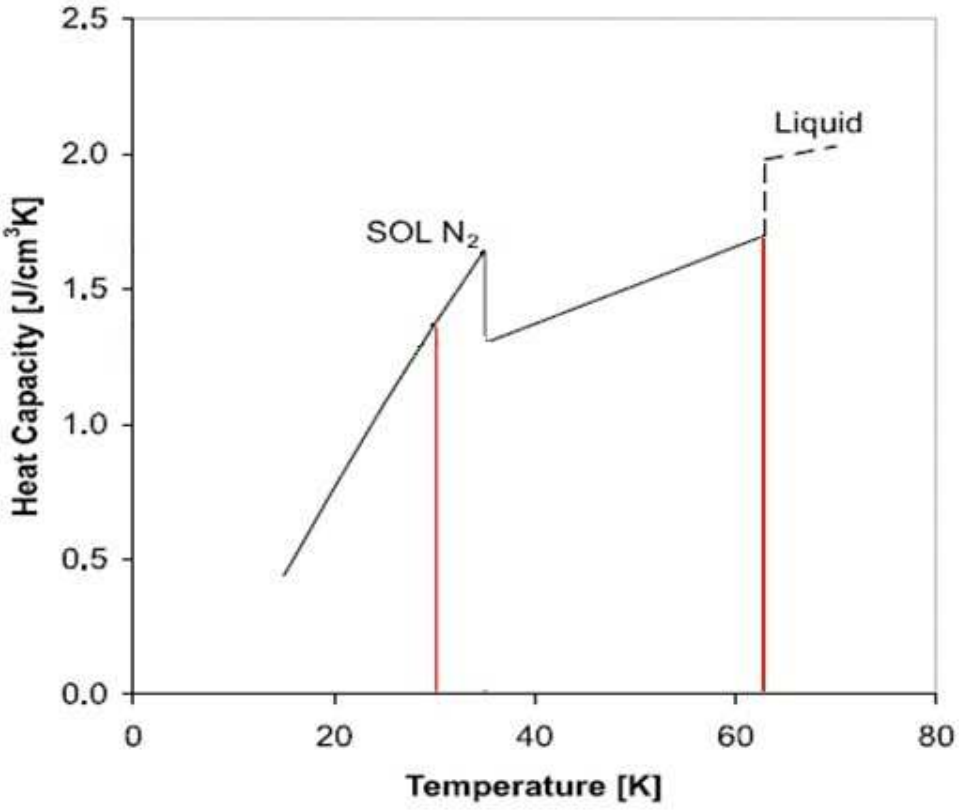

Figure A. 1 Volumetric Heat Capacity for Nitrogen [5]

Table A. 1, Table of Latent Heats for Nitrogen

	Volumetric Latent Heat (J/cm^3)	**Temperature (K)**
Vaporization	206.6	77.35
Fusion	26.7	63.15
Alpha-beta Phase Change	8.208	35.6

Integrating the volumetric heat capacity curve and accounting for the relevant latent heats yields the following between the temperatures of 30 K and 63.15 K:

$$Total\ Enthalpy\ Change_{30K\ to\ 63.15K} = \int_{30K}^{63.15K} C_p(T)dT = 83.9 J/cm^3$$

A.2 Argon

The volumetric heat capacity of argon is calculated similarly to that of nitrogen. Once more it is taken in the temperature range of 30 K to argons melting point (83.81 K).

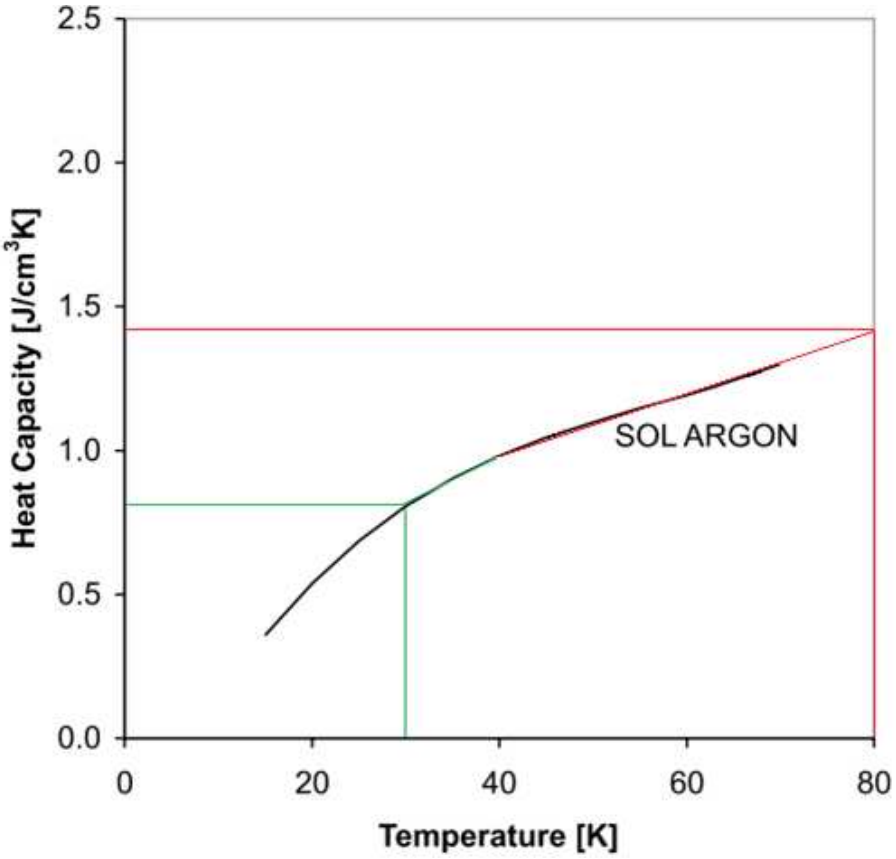

Figure A. 2 Heat Capacity for Argon [5]

Integrating the volumetric heat capacity curve and accounting for the latent heat of fusion yields the following between the temperatures of 30K and 83.81 K:

$$Total\ Enthalpy\ Change_{30K\ to\ 63.15K} = \int_{30K}^{83.81K} C_p(T)dT = 113.61 J/cm^3$$

Appendix B – Technical Data

B.1 Latent Heats for Common Cryogens

Table B. 1 Latent Heat of Vaporization for Common Cryogens [12]

	He^4	H_2	Ne	N_2
Boiling Point (K)	4.23	20.27	27.10	77.35
Latent Heat of Vaporization (J/g)	20.75	445.2	85.75	199.2